IEEE Access
Multidisciplinary | Rapid Review | Open Access Journal

Received May 23, 2019, accepted June 3, 2019, date of publication June 6, 2019, date of current version June 19, 2019.

Digital Object Identifier 10.1109/ACCESS.2019.2921335

Network Flow Dynamics Modeling and Analysis of Arrival Traffic in Terminal Airspace

LEI YANG[1], SUWAN YIN[2], AND MINGHUA HU[1]
[1]College of Civil Aviation, Nanjing University of Aeronautics and Astronautics, Nanjing 211106, China
[2]Department of Civil and Environmental Engineering, Imperial College London, London SW7 2BU, U.K.

Corresponding author: Lei Yang (laneyoung@ nuaa.edu.cn)

This work was supported by the National Natural Science Foundation of China under Grant 61573181 and Grant 71731001.

ABSTRACT This paper reveals and explores the flow dynamics of arrival traffic in a terminal airspace network on both mesoscopic and macroscopic levels in a systematic way from empirical data to dynamics modeling. The existence of link-based typical fundamental diagram (FD) that expresses the fundamental relations of newly defined flow-density-speed and network-based arrival macroscopic fundamental diagram (MFD-A) that represents aggregate demand-supply dynamics is demonstrated using empirical data collected in Guangzhou Terminal Airspace. After establishing heterogeneous FDs for flows along a different route segments using piecewise approximation, a density-speed-based modified cell transmission model (MCTM) is developed to simulate the spatio-temporal evolution of flow and congestion in arrival network for the enhancement of the adaption to non-uniform cell length and unique speed profile in terminal airspace. To further improve the simulation accuracy without compromising computational time, hybrid simulation is designed by deploying a queuing inspector (QI) to MCTM. The proposed network flow model is shown to be an efficient and accurate method capable of capturing the flow evolution at mesoscopic and macroscopic levels and supporting air traffic flow prediction and control. In the end, characteristics of arrival flow dynamics, including hysteresis, critical steady state (CSS), critical unsteady state (CUS), and its acceptable duration are discussed in depth as crucial theoretical parameters for air traffic flow management. This study provides a novel perspective method to model and understand the evolution of air traffic flow, and underpins advanced technical potentials for future air traffic management.

INDEX TERMS Terminal airspace, arrival traffic, network flow modeling, flow dynamics.

I. INTRODUCTION

Worldwide ATM system is undergoing the process of upgrading and transformation to cope with increasing air traffic demand and congestion especially in high-density airports and surrounding airspaces. Essentially, similar to the communication network, road traffic, production process and many more, air traffic congestion is generated due to the competition between users of limited resource, also known as the ''demand-supply'' imbalance, typically occurs during peak hours and in bottleneck situations, manifesting as the decline of traffic flow in the form of ground delay, speed reduction, detour, and even airborne holding. Within the strategic planning of ATM systems like SESAR, NextGen and ASBU, numerous advanced operational concepts, e.g. ''ATM Network Management'', ''User Driven Prioritization Process'', ''Flow Contingency Management'' and ''Complexity Management'', are proposed to enhance the system-wide performance and reduce the propagation of congestion. In order to develop and deploy high-level operational concepts and automation systems in an effective way, it is essential to conduct an in-depth investigation of the intrinsic air traffic dynamics by revealing temporal-spatial evolution and its underlying mechanism of air traffic flow characteristics.

The key to the study of traffic dynamics is to develop appropriate models and metrics that represent the generation, accumulation, propagation, and dissipation behavior of traffic congestions. In air traffic domain, though word ''flow dynamics'' has not been widely reported, relative researches have been done for decades starting by discussing about the delay and capacity since the 1940s [1], [2]. Currently, the two mean-based lines of studying air traffic flow dynamics are empirical analysis and flow dynamics modeling.

The associate editor coordinating the review of this manuscript and approving it for publication was Chaoyong Li.

Empirical studies covers a wide range from microscopic to macroscopic perspective. At detailed level, studies are focused on the exploration of prevailing flow patterns and their dynamic performance by analyzing trajectory data of aircraft. Levy [3] firstly developed a Normalized Cross-Track Distance metric to extract the 3D features of flight trajectories and further to identify typical and high-efficiency streams of traffic in terminal airspace. Recently, a number of clustering methods were proposed to refine the trajectory analysis method to generate a clearer picture of temporal-spatial distribution of flows, like K-Means [4], DBSCAN [5], Fourier Descriptor with Kernel Density Estimation [6] and Spectral Clustering [7], etc. Above trajectory analysis mainly studies the configuration of traffic flows and provide basis for airspace behavior monitoring and prediction rather than discussing the relationship between flow pattern transitions and congestion situations. Xu *et al.* [8] analyzed flow similarities, and quantified relations of flow rate, density and speed of air traffic flow along a high density route segment in terminal airspace. Three phase were identified as free flow, weak controlled flow and strong controlled flow. This initial attempt provide a new perspective on flow dynamics analysis although flow metrics are not fully capable of capturing the maneuvering features of terminal air traffic.

The development of complexity science carries ATM research to a brand new road. Deals of complexity metrics based on empirical radar data emerged to characterize the high-level situation of air traffic operation including flow states and air traffic controllers' cognition complexity. Classic metrics include Static Density [9], Dynamic Density [10], Tactical Load Smoother [11], Input-Output [12], Lyapunov exponent of trajectory dynamics [13], and Solution space-based metrics [14]. However, such studies mainly focus on the evaluation of air traffic situation objectively comparing to empirical workload rating or other well-accepted models, rather than exploring the dynamic evolution and intuitive relationship between complexity and congestion.

To quantify and analyze the air traffic flow congestion and it underlying mechanism by enrich all possible operational scenarios, traffic flow modeling presents its unique advantage. Queuing model as one of the earliest model is now widely used to model airport, terminal airspace and en-route operation to study the delay and capacity problems [15]–[16]. As the expansion of airport network and the urgent requirement of large-scale flow management, queuing network models were developed in both deterministic [17] and stochastic [18] way. Pyrgiotis *et al.* [19] discussed the system-wide effects of congestion using Approximate Network Delays Model that operates by iterating between its two main components: a queuing engine and a delay propagation algorithm at macroscopic level. Queuing models generally assume that the maximum throughput of subcomponent (e.g., route segment, navigation fix) in the airspace network maintains some pre-defined capacity in congestion, which is usually true in light congested situation. However, recent empirical studies [20] at airport surface suggested that the maximum runway departure rate would decrease as taxiing-out aircraft fall into severe congestion.

The flow dynamics of vehicle traffic have motivated many air traffic flow models in recent years, in order to predict the aggregate effect on air traffic delays and to support national-scale flow management. Bayen *et al.* [21] introduced partial differential equations [22] to the prediction of air traffic flow propagation, and the control of air traffic flow along one-dimensional air-routes in National Airspace Networks. Inspired by the Cell Transmission Model (CTM) [23]–[26] and Dynamic Network Loading (DNN) models [27]–[30] of vehicular traffic, 1D and 2D cell network models were derived by discretizing the partial differential equations. Building on the models developed by Menon *et al.* [31], [32], Large-capacity CTM was proposed by Sun and Bayen [33] and Wei *et al.* [34] to model large-scale air traffic networks by distinguishing link and cell levels for each flight path. Cao and Sun [35] developed a Link Transmission Model without discretization on the cell level to improve computational efficiency. Zhang *et al.* [36] proposed an analytical CTM-based flow model for terminal airspace by assuming that flow rate is a monotone non-decreasing function of density along route segments (or links). The primary focus of the abovementioned studies is the control of air traffic based on airspace or route capacity, with little attention given to the characterization or validation of the demand-supply dynamics describing the evolution of air traffic flow congestions, which plays a vital role in understanding the aggregate behavior of air traffic and is essential to the effectiveness of such controls. Recently, an efficient modeling approach based on the CTM was proposed for simulating the spatio-temporal evolution of flow and congestion on airport taxiway and apron networks based on empirical fundamental diagram that expresses the functional relationship between density and flow at link level [37]. Inspired by the concept of Macroscopic Fundamental Diagram (MFD), e.g. Daganzo [38]; Geroliminis and Daganzo [39]; Buisson and Ladier [40] and many others, and some prominent MFD-based traffic control [41]–[44], a proved MFD family of airport departure traffic for each arrival scenario was utilized to devise several robust off-block control strategies under uncertainties without referring to the complete evolution of congestion including formulation, accumulation and dissipation phases.

In addition, far more fine-grained simulation models of air traffic operations have also been developed. ACES, the Airspace Concept Evaluation System [45] and FACET, the Future ATM Concepts Evaluation Tool [46] both used currently by NASA and the FAA as microscopic and agent-based models. These kinds of simulation models guarantee high fidelity of air traffic flow but requires extensive model preparations and long computational time.

As a summary of the literature review above, existing studies mainly focused on the air traffic modeling, evaluation and optimal control, without many efforts to capture flow dynamics to understand the comprehensive characteristics of air traffic particularly in terminal airspace. In this paper, we try

to systematically explore the dynamic evolution patterns of arrival traffic flow, which is the most complex component in terminal airspace, by introducing a data-driven modeling using an adaptation of the CTM. It is noted that it is feasible to study arrival flows in terminal airspace independently to the departures due to that the physical (lateral or vertical) isolation of arrival and departure routes is generally guaranteed in flight procedure design and operation for potential risk avoidance (although exceptions may exist but not considered in this paper). The main contributions of this paper are summarized as follows:

(1) [Empirical FD and MFD-A]. We introduced a typical air traffic flow-density-speed Fundamental Diagram (FD) [47] at route segment (i.e., link) level for arrival traffic. A more detailed phases transitions from free to congestion are identified compared to [37]: free-flow, smooth, semi-stable and congested. At network level, Macroscopic Fundamental Diagram for Arrival (MFD-A) is revealed, capturing ''demand-supply'' dynamics and ''arrival-departure'' interactions.

(2) [Hybrid modeling of network flow dynamics]. To cope with the unique features of speed profile during arrival, a density-speed based CTM based on heterogeneous FDs is proposed to accommodate non-uniform cell length. All types of cell connections including simple connected, merge, diverge, crossover and runway are modeled. In order to address the problem of determining turning ratios for diverge connections in highly dynamic traffic patterns, a hybrid framework of mesoscopic network modeling is developed by introducing a ''First-In-First-Out'' queuing model to track and update the flights in cells to improve simulation accuracy without compromising computational efficiency.

(3) [Characteristics of arrival flow dynamics]. Based on the well calibrated and validated Modified-CTM (MCTM), the full pictures of congestion evolution consists formulation, accumulation and dissipation under various inflow level are presented. The conditional emergence of ''hysteresis'' is uncovered similar to clockwise loop of MFD [48], [49] in road network. In addition, two critical states named as Critical Steady States (CSS) and Critical Unsteady States (CUS) which are crucial references for air traffic flow management are discussed in depth at different level of departure demand.

The MCTM-based mesoscopic network model is sufficiently general to support a wide range of tasks involved in the design, planning, and operation of terminal airspace. It captures realistic approaching traffic dynamics such as free-flow, trailing, queuing, and holding, with intuitive parameters and rules. Its computational efficiency over microsimulation would make it an attractive modeling platform for air traffic research. The general flow dynamics and critical states explored in this paper provide theoretical background and solid basis to underpin the foundations of air traffic flow management from strategic to tactical stage.

The rest of this paper is organized as follows. Section II presents empirical network flow dynamics of arrival traffic in Guangzhou terminal airspace by establish typical FD and MFD-A. In Section III, we develop a modified cell transmission model of arrival network traffic by constructing a generalized configuration of fundamental diagram for heterogeneous flows along each route segment. We show the details of calibration and validation for MCTM by its modeling accuracy and efficiency in Section IV. To further uncover the arrival flow dynamics at theoretical level, some crucial characteristics are discussed in Section V. Finally, some conclusions are provided in Section VI.

II. EMPIRICAL NETWORK FLOW DYNAMICS OF ARRIVAL TRAFFIC IN TERMIANL AIRSPACE

A. DATA DESCRIPTION

Guangzhou terminal airspace is mainly responsible for the inbound and outbound traffic of Baiyun International Airport which is the top three busiest airport in China. Considering the maneuvering activities which are the main operational feature of terminal air traffic, two types of original data are collected: Static Route Network and Discrete Radar Trajectory from 11/09/2015 to 17/09/2015.

Static Route Network. Routes segments (or links) connected by navigation fixes constitute static and basic structure of route network in terminal airspace. To provide air traffic service in a safe and efficient manner, standard flight procedures are designed as background knowledge for air traffic controllers and pilots. Each standard route consists of a series of adjacent links guiding flights from TMA (Terminal Maneuvering Area) airspace entry points to the landing runway. Figure 1 (a) shows the route network of Guangzhou terminal airspace where most of arrival (green) and departure (red) air routes are physically isolated except for link SHL-IDUMA which is laterally shared by arrival and departure flows but vertically separated. Physical isolation of arrival and departure routes as one of the main features of terminal airspace structure, gives the opportunity to model arrival flow independently. However, runways are always the main shared resource for both arrivals and departures in mixed operation.

Discrete Radar Trajectory. A trajectory is a time-ordered sequence of 5-tuples representing the longitude, latitude and height coordinates, heading and horizontal speed of a flight at each snapshot time with a fixed time interval, as shown in Table 1. Due to the position uncertainty of hand-over from upstream en-route sector, and maneuvering actions guided by air traffic controllers, the operational trajectories have certain deviation from standard route segment as shown in Figure 1(b).

In order to analyze the network flow dynamics of traffic flow, the very first and vital step is to identify the spatial subordination relationship between route segment and discrete trajectory points. While projecting a trajectory to the nearest route segment has been widely adopted in practice, this method could lead to erroneous mappings such as the one illustrated in Figure 2. In this figure, trajectory point p^{j+2} would be mapped to link B-C following the

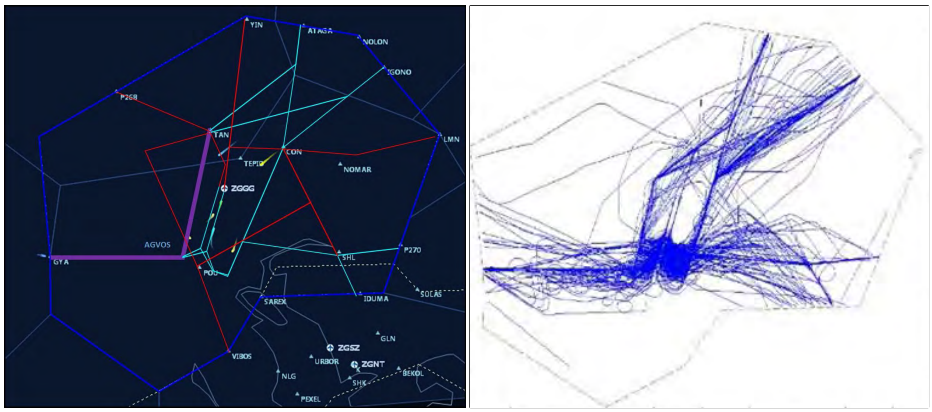

(a) (b)

FIGURE 1. Data visualization of Guangzhou terminal airspace. (a) Airspace configuration (green: Standard arrival routes, red: Departure routes, purple: Merge routes of GYA-AGVOS and TAN-AGVOS). (b) Trajectories of arriving flights on a sample day.

TABLE 1. The sample of discrete radar trajectory data for flight FDX34.

Snapshot time	Flight number	Latitude	Longitude	Altitude (ft)	Ground Speed (Knots)	Heading(degree)
21:45:10	FDX34	23.069	112.8895	7900	457	91
21:45:25	FDX34	23.06605	112.9083	7500	443	117
21:45:40	FDX34	23.05848	112.9219	7300	446	116
21:46:55	FDX34	23.04354	112.9450	6900	456	121
21:46:10	FDX34	23.04048	112.9504	6900	455	119
21:46:25	FDX34	23.02832	112.9726	6900	452	119
21:46:40	FDX34	23.01784	112.9914	6900	452	119
21:46:55	FDX34	23.00973	113.0064	6900	454	118
21:47:10	FDX34	22.99883	113.0266	6900	456	119

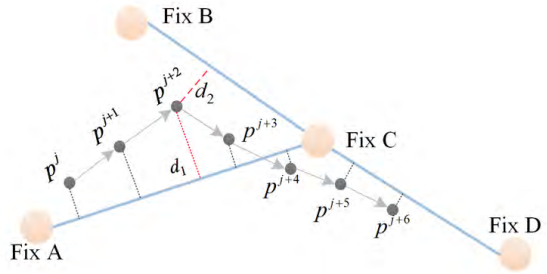

(a)

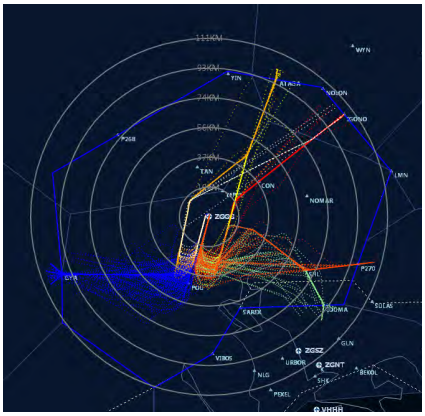

(b)

FIGURE 2. Schema of standard route segment and flight trajectories. (a) Deviations of trajectory points. The distance between trajectory point and standard route segment is indicated as the lengths of the dashed line segment, i.e. the Euclidean distance from a point to a line segment; (b) "Trajectory-Route Mapping" result for arrival flows in terminal airspace of ZGGG (Different colors stand for different trajectory clusters consistent with standard flight routes).

minimum-distance rule as $d_1 > d_2$, while in fact the continuity of the trajectory dictates that p^{j+2} should be mapped to link A-C. In order to remedy such a deficiency, we adopt a more robust "Trajectory-Route Mapping" algorithm [50]

that maps the flight trajectories to the route segment, thereby establishing, while maintaining the consistency of the flight routes. Figure 2 (b) demonstrates the clustering result of arrival flow based on the network structure and trajectory data described in Figure 1, which provides essential data for further empirical analysis on arrival flow dynamics in Section II.B.

B. EMPIRICAL NETWORK FLOW DYNAMICS OF ARRIVAL TRAFFIC

1) FUNDAMENTAL DIAGRAM (FD) OF ARRIVAL FLOW AT LINK LEVEL

Fundamental Diagram presents the basic flow dynamics by illustrating the relations among flow rate, density and velocity of traffic flow at link level. Unlike road traffic operation, air traffic in terminal airspace presents unique characteristics influenced by ATCOs. When congestion occurs in the terminal airspace, maneuvering commands, including speed reduction, detour, and hold are issued to change pre-planned route to avoid potential conflicts. For the unique features of arrival flow, modified definitions of fundamental parameters were defined.

- ***Average Flow Rate*** (AFR) $\overline{q_r}(\tau)$. AFR is the average outflow rate from link r during time period τ.
- ***Equivalent Average Density*** (*EAD*) $\overline{\rho_r}(\tau)$. EAD is defined as the reciprocal of average distance between contiguous aircraft on the same link during time period τ. At any snapshot time $t \in \tau$, total amount of aircraft denoted as M_r^t are travelling along link r. The horizontal coordinate of tail point of link r and flight $m \in F$ at t is denoted as $p_r(x, y)$ and $p_m^t(x, y)$ respectively. Then EAD is formulated in equation (1) and (2).

$$\overline{\rho_r}(\tau) = \frac{1}{N} \sum_{t \in \tau} \overline{\rho_r}(t) \tag{1}$$

$$\overline{\rho_r}(t) = \begin{cases} \dfrac{M_r^t - 1}{L_t^{max} - L_t^{min}}, & if\ M_r^t > 1 \\ M_r^t / L_r, & otherwise \end{cases} \tag{2}$$

where $L_t^{max} = \max dist(p_r(x, y), p_m^t(x, y)), m \in$ is the furthest Euclidean distance between aircraft and tail point of link r, while L_i^{min} is the nearest distance calculated similarly; L_r is the length of link r; N is the number of snapshots during τ.

- ***Equivalent Average Speed*** (EAS) $\overline{v_r}(\tau)$. EAS is the average effective speed of aircraft travelling along route segment during time period τ. At any snapshot time $t \in \tau$, the instantaneous speed of flight m flying along link r is denoted as $v_r^m(t)$. EAS is capable of characterize a series of actions taken by pilots, like acceleration, deceleration, rerouting (path stretching or shortcut), and even holding, according to the air traffic controller's intervention or standard flight procedures, as formulated in equation (3).

$$\overline{v_r}(\tau) = \frac{1}{N} \sum_{t \in \tau} \frac{1}{M_r^t} \sum_{m \in F} \left\| v_r^m(t) \right\| \cdot \Im_r^m \tag{3}$$

where $\left\| v_r^m(t) \right\|$ is the Actual Velocity Scalar (AVS) of aircraft m at snapshot time t; $\Im_r^m$ is the Velocity Gain Coefficient (VGC) of aircraft m along link r defined to be the ratio of the standard link length to the actual flying distance along link r.

- ***Nominal Flow Rate*** (NFR) $\overline{q_r^*}(\tau)$. According to the "fundamental equation" [44] of road traffic flow, $\overline{q_r^*}(\tau) = \overline{\rho_r}(\tau) \times \overline{v_r}(\tau)$.

To capture complete phase states of air traffic flow and to further establish fundamental diagram, we provide an illustration using the largest traffic flows traveling along the merge links GYA-AGVOS and TAN-AGVOS, which are highlighted by purple in Figure1(a). It is noted that, in merging scenarios, the flow along each link can be regarded as one. Figure 3 (a) and (b) show the non-linear configurations of AFR and EAS evolve with EAD respectively. Generally, as EAD increases, more intense constraints among aircraft lead to decreased EAS to varying degrees, while the EAD-AFR relationship exhibits a concave shape with close-to-linear increase of the flow for relatively low density. These observations reveal similar patterns in road traffic [51], [52]. Moreover, Figure 3 (c) demonstrates the high consistency (slope ≈ 1) between AFR and NFR providing a strong basis for density-speed network flow modeling in next section. For detailed analysis of arrival flow dynamics at link level, with the additional help of flight data replay using SIMMOD simulator, four phases are divided by dissecting both fundamental diagram as shown in Figure 3 (a)-(b). In addition, the temporal-spatial diagram in Figure 3(d), which illustrates the speed and path changes by scattered trajectory points of individual aircraft along the merge routes, is adopted as a supplementary characterization of the flight maneuvering features in each phase state.

(1) **Free Phase**. Extremely low traffic density results in large spatial headways and little interactions among aircrafts. For the different speed profiles assigned to flights based on individual performance, the EAS presents significant fluctuation. As shown in Figure 3 (d), shortcut strategies observed by flight distance reductions and higher velocities denoted by the slopes of temporal-spatial trajectories also increase the flow efficiency.

(2) **Smooth Phase**. EAS is relatively high with a slight decrease due to occasional conflicts. AFR increases linearly as EAD grows. At this period, aircraft are lined up in standard flight route with approximately equal flight distance observed in Figure 3 (d), though the spatial headways are not even. Air traffic flow is at its best and stable operational status

(3) **Semi-stable Phase**. Aircraft are still flying along standard route with closer and more uniform spatial headways as shown in Figure 3 (d). EAS is still at an upper-middle level though a noticeable decrease appears due to rising conflicts solved mainly by speed reduction and occasional

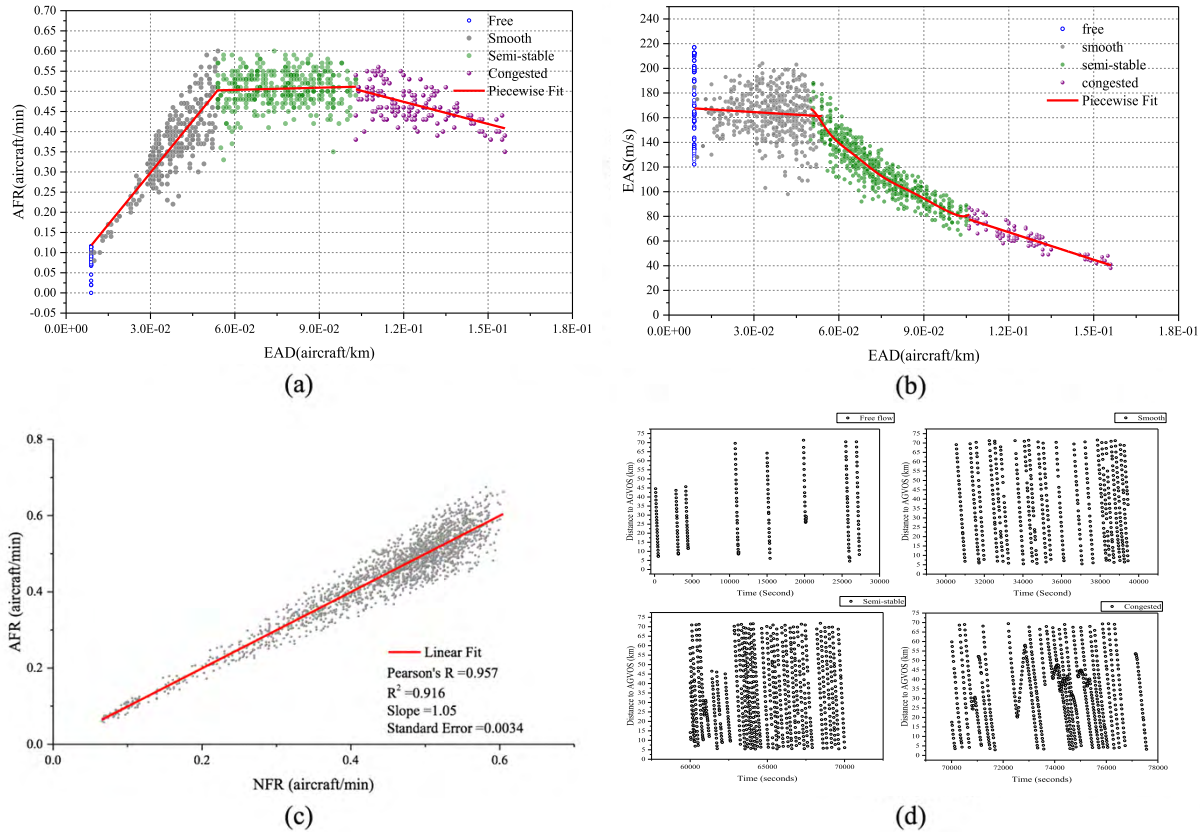

FIGURE 3. Typical fundamental diagram configuration of link-based arrival flow. (a) Basic phase state implied in flow evolution presented by EAD-EAS relationship; (b) Basic phase state implied in flow evolution presented by EAD-AFR. (c) Correlation between AFR and NFR. (d) Temporal-spatial diagram of air traffic flow along merge routes GYA-AGVOS and TAN-AGVOS.

heading change. The AFR reaches and maintain the maximum when EAD moves to the critical value. Though airspace resource is in its full usage condition, the traffic state is not stable and phase transition may easily occur when disturbed.

(4) **Congested Phase.** EAS and AFR continuously drop as density increases. From microscopic view, the resolution of conflict turns from speed strategy to radar vectoring even holding as shown in Figure 3 (d). From macroscopic view, the streamline of traffic changes from structured linear state into disseminative planar state. Besides, the difficulties of calculating parameters of radar vectoring and holding like outbound angle, holding time, etc. by human brain is also a primary reason that leads to inefficient use of resource capacity.

As we can see in Figure 3(a)-(b), 0.05aircraft/km and 0.1aircraft/km are critical density of phase transition from smooth to semi-stable, and from semi-stable to congestion, respectively. Interestingly, the controlled separation and minimum separation along these two routes are 15km and 10km respectively according to air traffic control operation regulation of Guangzhou terminal airspace. It is noted that, based on the definition of EAD, the situation that traffic density is higher than 0.1 aircraft/km doesn't imply any conflict occurs. Aircraft still maintain lateral or vertical minimum separation by radar vectoring.

2) EMPIRICAL MACROSCOPIC FUNDAMENTAL DIAGRAM (MFD) OF ARRIVAL FLOW AT NETWORK LEVEL

We extend the fundamental diagram from link level to the system-wide network level to explore the high-level "demand-supply" dynamics for characterizing network flow congestion evolution. Macroscopic Fundamental Diagram (MFD) in urban network well describes the "demand-supply" dynamics by linking between network vehicle density (or accumulation) and network space-mean flow (or trip completion flow) [39]–[40]. Inspired by previous studies on MFD, we define MFD-Arrival (MFD-A) to characterizes the aggregate behavior of the arrival network in terms of occupancy (arrival demand) and outflow (landing rate), in a parsimonious way yet capable of capturing the key demand-supply relationship in a more intuitive way. We define the following key quantities:

- ***Arrival Demand (AD)*** is the number of arrival aircraft in terminal airspace at some time instant.
- ***Landing Rate (LR)*** is the number of aircraft landing on the runway during a given unit time.
- ***Departure Rate (DR)*** is the number of aircraft departing from the runway during a given unit time.
- ***Critical Arrival Demand (CAD)*** is the minimum arrival demand that maximizes the Landing Rate.

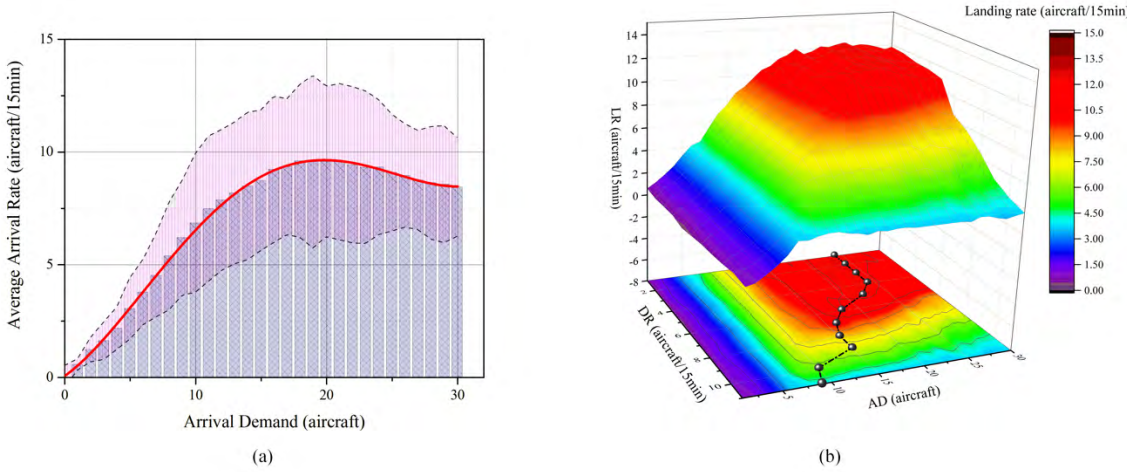

FIGURE 4. Macroscopic fundamental diagram of arrival network flow. (a) Average arrival rate under different demand. (b)Impact of departure rate on MFD-A.

Figure 4 (a) shows the average MFD-A, representing the relationship between arrival demands and landing rate. The bars show the average while the shaded area indicates standard deviation. The Pearson correlation test indicates a high positive correlation of 0.827 between AD and LR; the two-tailed probability passes the significance level test at 0. It is widely accepted in air traffic operation that the system throughput continuously rises with increasing demand until a certain point where the system reaches its maximum capacity. However, our result shows a slight drop of LR after passing the critical arrival demand. The main reason is that the speed reduction may lead to the expansion of the headway between successive arrivals in congested network. Moreover, this is also partially attributed to the workload of ATCOs in dealing with complex situations, which generally causes larger separation buffers between aircraft, resulting in lower utilization of network capacity.

Figure 4(b) shows the impact of runway departure rate on MFD-A. The MFD-A is not sensitive to the lower departure rate as the CADs and LRs don't show any differences. This can be explained by the runway capacity envelop configuration [53], as shown in Figure 8(b). When the runway departure rate continuously increasing, the average arrival rate decreases noticeably due to the competition for runway resource. Meanwhile, the identified CAD drops as well, shown by the dots in Figure 4(b).

III. ARRIVAL FLOW MODELING BASED ON MODIFIED-CTM

A. PIECEWISE APPROXIMATION OF GENERALIZED FUNDAMENTAL DIAGRAM

The cell transmission model is a widely used mesoscopic traffic flow model, which is based on the Godunov discretization of the well-known Lighthill-Whitham-Richards kinematic wave model [22]. Traditional CTM is based on a trapezoidal or triangular fundamental diagram, and propagates flow and

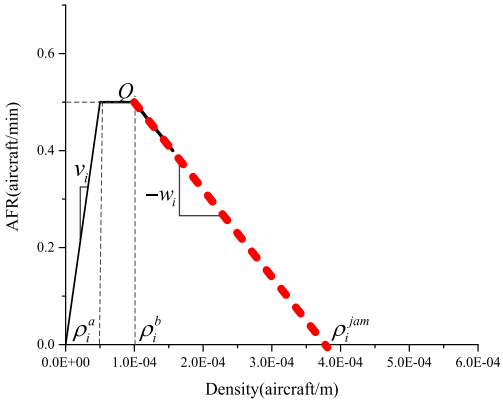

FIGURE 5. Generalized fundamental diagram of arrival flow in terminal airspace.

congestion between cells by straightforward bookkeeping, which admits efficient computation for large and complex networks. As suggested by phase transition pattern and representative fundamental diagram, we give the hypothesis that arrival flows along different route segments (links) are complied with the similar trapezoidal configuration of fundamental diagram (see Figure 5) but heterogeneous in critical parameters defined as follows.

- $\rho_i^a = 1/1000d_i$(unit: aircraft/m), is the critical density of phase transition from smooth to semi-stable, and is determined by Coordinated Separation (CS) of route i denoted as d_i in kilometers (km). Here, CS is defined as a regulated separation criteria adopted by controllers in some sector according to the hand-over agreement with downstream sectors.
- $\rho_i^b = 1/1000S$(unit: aircraft/m), is the critical density of phase transition from semi-stable to congested, which is determined by separation minimum of route i denoted by S (km) according to operation regulations.

- $Q_i = v_i \Delta t / 1000 d_i$(unit: aircraft/min), is the maximum outflow of route i during a certain period Δt(s), which is determined by d_i and average speed v_i (m/s) in free and smooth phase.
- w_i(unit: m/s)is the propagation speed of congestion wave along route i. It is one of the most critical parameters that presents congestion evolution.
- ρ_i^{jam}(unit: aircraft/m) is the jam density of route i, which may be impossible to occurs in real-world air traffic operations. It is determined as the intersection of x-axis and line (as shown by the red dot line in Figure (5) which passes point Q_i at ρ_i^b with a slop of $-w_i$. Since we cannot observe the drop of AFR, we assume that jam density is uniform across all routes in the terminal airspace. Therefore, w_i of each route segment can be ideally determined by Q_i and ρ_i^{jam}.

Then the flow rate of any route segment in different flow states can be derived as follows:

$$q(\rho) = \begin{cases} \rho v_i, & \rho \in [0, \rho_i^a) \\ Q_i / \Delta t, & \rho \in [\rho_i^a, \rho_i^b] \\ w_i \left(\rho_i^{jam} - \rho\right) / \Delta t, & \rho \in (\rho_i^b, \rho_i^{jam}] \end{cases} \quad (4)$$

In other words, the EAS in different flow states is derived as

$$v(\rho) = \begin{cases} v_i, & \rho \in [0, \rho_i^a) \\ Q_i / \rho \Delta t, & \rho \in [\rho_i^a, \rho_i^b] \\ w_i \left(\rho_i^{jam} - \rho\right) / \rho \Delta t, & \rho \in (\rho_i^b, \rho_i^{jam}] \end{cases} \quad (5)$$

B. MCTM-BASED ARRIVAL FLOW MODELING

Compared to road traffic, arrival traffic in terminal airspace has its unique features. The most crucial one in mesoscopic flow modeling is the speed profile along each route segment. Generally, different speed range (i.e., free flow speed and minimum speed) constrained by height limitation regulated in standard flight procedures is assigned to each route segment during approach. Although certain speed overlap exists between adjacent links, ground speed of any arrival aircraft is non-increasing. That means, any flight that enters into a downstream link with a slower speed is generally not allowed to accelerate to keep pace with leading aircraft. Since the maximum speed along different route segment is heterogeneous, according to Courant-Friedrichs-Lewy (CFL) condition [54], it would not be possible to divide each route segment into cells with equal length while ensuring the same modeling resolution. Here we develop a density-speed based CTM similar to [47] except that we use densities as state variables instead of occupancies to accept non-uniform cell length.

In the rest of the section, four types of ordinary cells, including simple connection, merge, diverge and crossover cells decomposed from arrival network shown in Figure 6, and runway cells are detailed modeled. We consider the time increment Δt such that the CFL condition holds for each cell:

$$l_i \geq v_i \times \Delta t$$

where v_i denotes the free-flow speed of the cell. The following notations are used in this paper.

v_i :	Forward wave speed (free-flow speed) of cell i;
w_i :	Backward wave speed of cell i;
Q_i :	Maximum number of aircraft that can be transmitted through cell i within one time step
C_M	Capacity of fix M
$\rho_i(t)$:	The traffic density of cell i at the beginning of time step t
$n_i(t)$:	The number of aircraft in cell i at the beginning of time step t, $n_i(t) = \rho_i(t) \times l_i$
$y_i(t)$:	The number of aircraft entering cell i from its upstream cell $i-1$ during time step t
$v_i(t)$:	The average EAS of cell i during time step t
ρ_i^{jam} :	The jam density of cell i
l_i :	The length of cell i
Δt :	The time increment
v_i^0 :	The regulated lower bound of flying speed in cell$i$

1) ORDINARY CELLS

(a) Simple connection. If two cells are connected to one another without any intervening as shown in Figure6 (b), then the cells are said to be simply connected. Let i-1 be the upstream cell and i be the downstream cell in the pair. The fundamental recursion that propagates flow between simple connection cells is expressed as (6), as shown at the bottom of the next page.

The first equation is a simple statement of flow conservation; the second one presents the flow transmission between adjacent cells and congestion propagation composed of demand and supply part of connected cells formulated as:

$$\begin{cases} D_{i-1}(t) = \min\{n_{i-1}(t), \rho_{i-1}(t) \times v_{i-1}(t) \times \Delta t\} \\ S_i(t) = \min\left\{C_M \times \Delta t, Q_i, w_i\left(\rho_i^{jam} - \rho\right) \times \Delta t\right\} \end{cases} \quad (7)$$

where demand is the maximum flow sent out from cell $i-1$ determined by current density and EAS; while supply is the maximum inflow can be accepted by cell i under congested conditions; C_M is the capacity of the fix between two cells (See Appendix A). And the third equation in Equation (6) is the Speed Transmission Function (STF) aims at calculating instantaneous average EAS of air traffic flow in cell i at the end of time step t, where $v_i^{in}(t)$ is the average AVS of inflow speed from cell i-1 to cell i and $v_i^{out}(t)$ is the average AVS of outflow of cell i formulated as:

$$\begin{aligned} v_i^{in}(t) &= \min\left(\max\left\{\frac{y_i(t)}{\rho_{i-1}(t) \times \Delta t}, v_{i-1}^0\right\}, v_i\right) \\ v_i^{out}(t) &= \max\left\{\frac{y_{i+1}(t)}{\rho_i(t) \times \Delta t}, v_i^0\right\} \end{aligned} \quad (8)$$

Different from that in traditional CTM, here we firstly propose *STF* to represent congestion propagation in

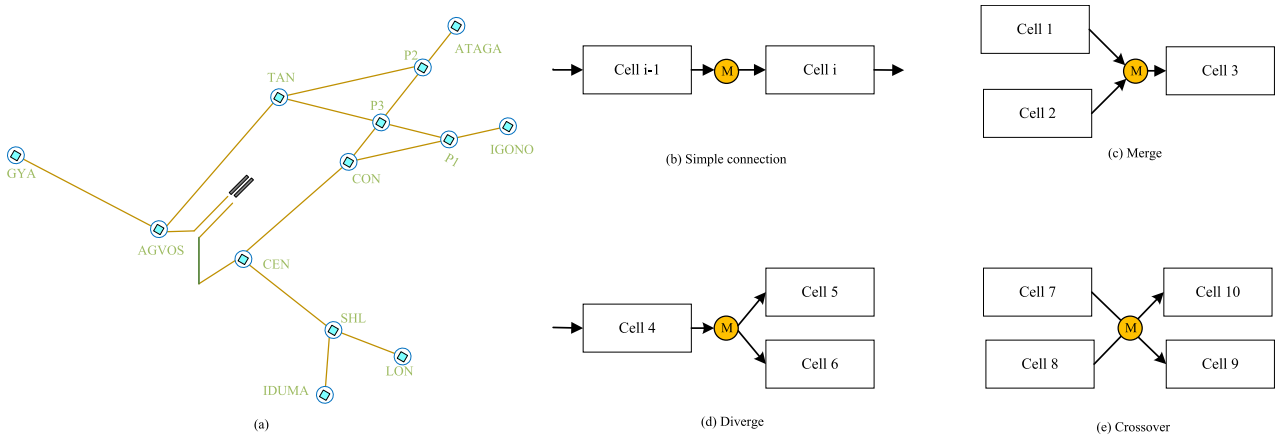

FIGURE 6. Network structure of arrival route in terminal airspace. (a) Arrival route of Guangzhou terminal airspace. (b-e) Ordinary cell configurations extracted from real world. No turning is allowed at crossover junction.

terminal airspace. In the following part of this section, junction scenarios (merge/diverge/crossover) are discussed. Since the *STF* is universal throughout the cell network, we only focus on the different flow transmission limitations of various configurations of junctions for the sake of simplification.

(b) Merge connection. A merge connection refers to most common situation during approaching that two or more route segments are connected to a single downstream link at the same fix as shown in Figure6 (c). We let $y_{1\to3}(t)$ be the number of aircraft transmitted from cell 1 to cell 3 during time step t; similar notations are used below with obvious meaning. The following demand and supply constraints apply:

$$\begin{aligned} &y_{1\to3}(t) \le D_1(t), y_{2\to3}(t) \le D_2(t), \\ &y_{1\to3}(t) + y_{2\to3}(t) \le S_3(t) \end{aligned} \tag{9}$$

In addition, we assume that flow coming from cells 1 and 2 receive different priorities, $p_1 > 0$ and $p_2 > 0$ such that $p_1 + p_2 = 1$. As a global manager, air traffic controller should ensure the equity of aircraft operations besides safety and efficiency. In merge scenarios, upstream route segment with more aircraft is normally assigned higher priority to avoid possible congestion accumulating on that link. Demand-based priority [55] is one of the best interpretations of above equity. The distribution fractions are only related to the demands $D_1(t)$ and $D_2(t)$, as defined in (10).

$$\begin{aligned} p_1 &= D_1(t)/(D_1(t) + D_2(t)) \\ p_2 &= D_2(t)/(D_1(t) + D_2(t)) \end{aligned} \tag{10}$$

As explained in Appendix A, the capacity of merge point is sensitive to the flow structure. To be consistent with the distribution fractions, the demand-based mathematical expectation of point capacity is defined in (11).

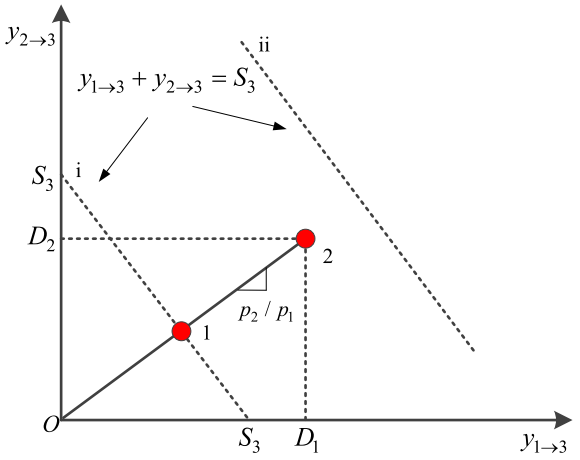

FIGURE 7. The schema of merging rule.

$$C_M = \sum_{i=1}^{2}\sum_{j=1}^{2} p_i p_j C_M^{i,j} \tag{11}$$

where $C_M^{i,j}$ is the capacity of point M when flights from cell j pass the fix following flights from cell i.

The merging rule is best explained using Figure 7. The solution of merging flow is uniquely determined by (12): the intersection of $y_{1\to3}(t) + y_{2\to3}(t) = S_3(t)$ and $p_1/p_2 = D_1(t)/D_2(t)$ when $D_1(t) + D_2(t) \ge S_3(t)$, and

$$\begin{cases} \rho_i(t+1) = \rho_i(t) + (y_i(t) - y_{i+1}(t)) \times \dfrac{1}{l_i} \\ y_i(t) = \min\left\{n_{i-1}(t), \rho_{i-1}(t) \times v_{i-1}(t) \times \Delta t, C_M \times \Delta t, Q_i, w_i\left(\rho_i^{jam} - \rho\right) \times \Delta t\right\} \\ v_i(t+1) = \min\left\{\dfrac{y_i(t) \times v_i^{in}(t) + (n_i(t) - y_{i+1}(t)) \times v_i^{out}(t)}{\rho_i(t+1) \times l_i}, v_i(\rho_i(t+1))\right\} \end{cases} \tag{6}$$

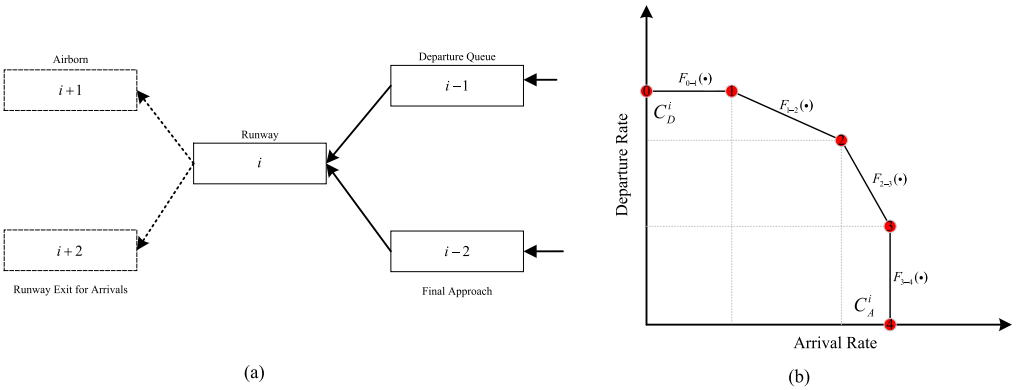

FIGURE 8. The network features of runway operation. (a) Cell network; (b) Capacity envelop of runway.

the point *2* otherwise.

$$\begin{cases} y_{1\to 3}(t) = \min\{D_1(t), p_1 \times \min(S_3(t), D_1(t) + D_2(t))\} \\ y_{2\to 3}(t) = \min\{D_2(t), p_2 \times min(S_3(t), D_1(t) + D_2(t))\} \end{cases} \tag{12}$$

(c) Diverge Connections. A diverge connection refers to another common situation during approaching that aircraft travelling along same route segment have different destinations as shown in Figure6 (d). In multi-runway operation, air traffic controllers select different landing runways for arrival flights to balance the runway throughput and reduce taxiing time at airport surface at the diverging fixes as shown by P1 and P2 in Figure6(a).

It is assumed that air traffic flow leaving cell 4 to cell 5 and 6 follows certain turning ratios $\sigma_{4\to 5} \geq 0$ and $\sigma_{4\to 6} \geq 0$ which sum up to be one. In review of (11) and flow maximization principle, following solution is derived:

$$\begin{cases} y_{4\to 5}(t) = \sigma_{4\to 5} \cdot \min\left\{D_4(t), \dfrac{S_5(t)}{\sigma_{4\to 5}}, \dfrac{S_6(t)}{\sigma_{4\to 6}}\right\} \\ y_{4\to 6}(t) = \sigma_{4\to 6} \cdot \min\left\{D_4(t), \dfrac{S_5(t)}{\sigma_{4\to 5}}, \dfrac{S_6(t)}{\sigma_{4\to 6}}\right\} \end{cases} \tag{13}$$

Note that the capacity of diverge fix is derived similar to that of merge connection. As a highly dynamic parameter, turning ratio in diverge cells is determined by standard routes that assigned to the aircraft in the cells. Generally, the route assignment by controllers is mainly based on flight plan and the concern of traffic load balance among sectors and runways. Traditional CTM is an aggregate flow model, it is not capable of tracing individual aircraft. To address this shortcoming, we develop a Queuing-based MCTM detailed in Section IV.A.

(d) Crossover Connections. A crossover connection refers to a common situation that two or more route segments cross each other at one or more fixes without turning[1] as shown in Figure6(e). The flow discharges from cell 7 and 8 are not only constrained by the supplies of respective upstream cells, but also the capacity of crossover fix shared by incoming approaches. Similar to merge connections, demand-based priority is adopted to derive the crossover capacity C_M and flow transmission in (14).

$$\begin{cases} y_{7\to 9}(t) = \min(D_7, \beta_{7\to 9} \times C_M \times \Delta t, S_9) \\ y_{8\to 10}(t) = \min(D_8, \beta_{8\to 10} \times C_M \times \Delta t, S_{10}) \end{cases} \tag{14}$$

where $\beta_{7\to 9} = D_7/(D_7 + D_8)$, and $\beta_{7\to 9} + \beta_{8\to 10} = 1$.

2) CELLS OF RUNWAY NETWORK

Runway is generally regarded as the main bottleneck of terminal air traffic operation. In many terminal airspace networks, runway serves as both sink for arrivals and source for departures as shown in Figure 8 (a). In contrast to how 2×2 intersections are typically modeled for vehicular traffic [56], the runway network has its unique characteristics. First, arrival traffic through cell *i*-2 has significant priority over departure traffic through cell *i*-1 when occupancy of cell *i*-1 is below its threshold denoted by Θ representing the maximum length of runway queuing. The capacity tradeoff for departure and arrival traffic is captured through the fundamental diagram of runway, also known as the envelope model as shown in Figure 8 (b). Here, we adopt a "Frequency-constraint Quantile Regression" (F-QR) method to refine the capacity envelope [57]. Such a system can be modeled as following set of equations of:

$$y_{i-2\to i}(t) = \min\left\{D_{i-2}(t), S_A^i(t)\right\} \tag{15a}$$

$$\begin{cases} S_A^i(t) = C_A^i \\ S_D^i(t) = F(y_{i-2\to i}(t)) \\ y_{i-1\to i}(t) = \min\left\{n_{i-1}(t), S_D^i(t)\right\} \end{cases} \quad \text{if} \Theta > n_{i-1}(t) \tag{15b}$$

$$\begin{cases} y_{i-1\to i}(t) = \min\left\{n_{i-1}(t), C_D^i\right\} \\ S_A^i(t) = F'(y_{i-1\to i}(t)) \end{cases} \quad \text{if} \Theta \leq n_{i-1}(t) \tag{15c}$$

where C_A^i and C_D^i are maximum arrival and departure rate, $F(.)$ is the piecewise linear functions of capacity

[1] If turning is allowed, then we have a 2-by-2 junction model, which can be treated in similar ways as the merge/diverge junctions. Due to space limitation, in this paper we do not perform an exhaustive discussion of different junction geometries, and instead refer the reader to [56] for a more extensive coverage.

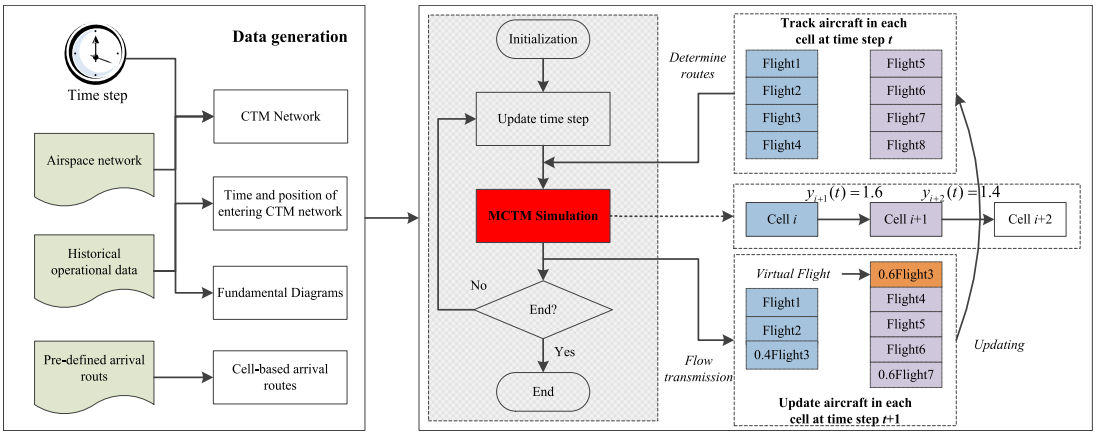

FIGURE 9. The hybrid framework of CTM-centered simulation.

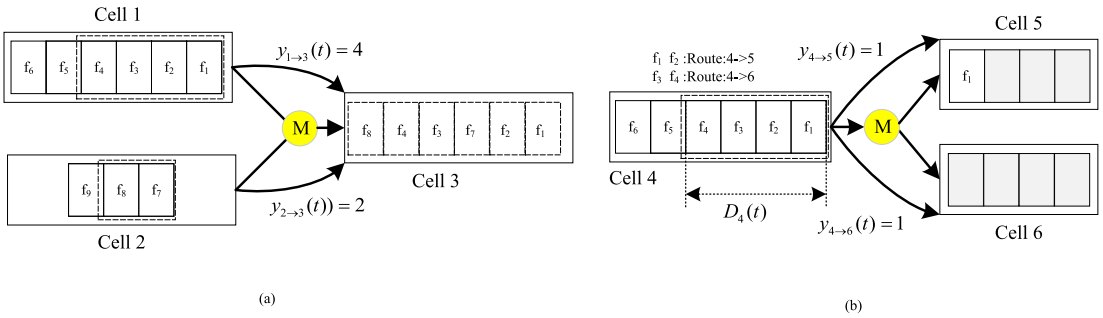

FIGURE 10. The mechanism of QI in merge and diverge scenarios. (a) Merge. (b) Diverge.

envelope as shown in Figure9 (b); $F^{'}(.)$ is the inverse function of $F(.)$.

IV. CALIBRATION AND VALIDATION OF MCTM OF ARRIVAL FLOW IN TERMINAL AIRSPACE

A. HYBRID FRAMEWORK OF QUEUING-BASED MCTM SIMULATION

Mesoscopic traffic models, which fill the gap between microscopic models that model and trace the behavior of individual vehicles and macroscopic models that describe traffic as a continuum flow, simulate individual vehicles or group of vehicles, but describe their activities and interactions based on aggregate (macroscopic) relationships [58]–[62]. As a mesoscopic traffic model, CTM ignores fine granularities and describes the aggregate behavior of travel agents in a robust and computationally efficient way. However, losing sight of individual aircraft will result in rough estimation of the turning ratio which is an essential parameter for determining temporal-spatial distribution of traffic flow. In road traffic, turning ratio is normal set manually or modeled as a dynamic network loading problem extensively studied in the dynamic traffic assignment literature [63]. Here, to improve simulation accuracy we proposed a hybrid approach called ''Queuing-based MCTM'' simulation (Q-MCTM) with the combination of a mesoscopic simulator (MCTM) and a microscopic Queue Inspector (QI) for tracking & updating aircraft queuing in cells in order to capture the highly time-varying parameters without compromising the efficiency.

Flights in terminal airspace are assigned by standard routes according to pre-determined flight plan. A Dynamic Flight List (DFL) is generated for each cell to store the queuing information of flights based on First-In-First-Out (FIFO) hypothesis. At the beginning of each time step, QI provides the flow direction discharged from each cell by analyzing the flight route of each aircraft in DFL and generate turning ratio especially for diverge cells. After running MCTM simulator for one time step, the DFL is update according to the flow transmission results. The framework of hybrid simulation is shown in Figure 9. It is noted that, although QI is working in non-integer principle, the ''virtual flight'' is ignored when calculating turning ratios since the flight is still in the upstream cell. In crossover scenarios, the update mechanism is simple and similar to that of simple connections. To make it clearly understandable, merge and diverge cells are taken as examples to demonstrate some unique working process of QI.

(1) Merge cells. During each time step, the priority p_1, p_2 and outflow of cell 1 and 2 are determined by Equation (9-12). Flights in cells inherit the priority of flows. As shown in Figure10(a), $y_{1\to3}(t) = 4$, and $y_{2\to3}(t) = 2$,

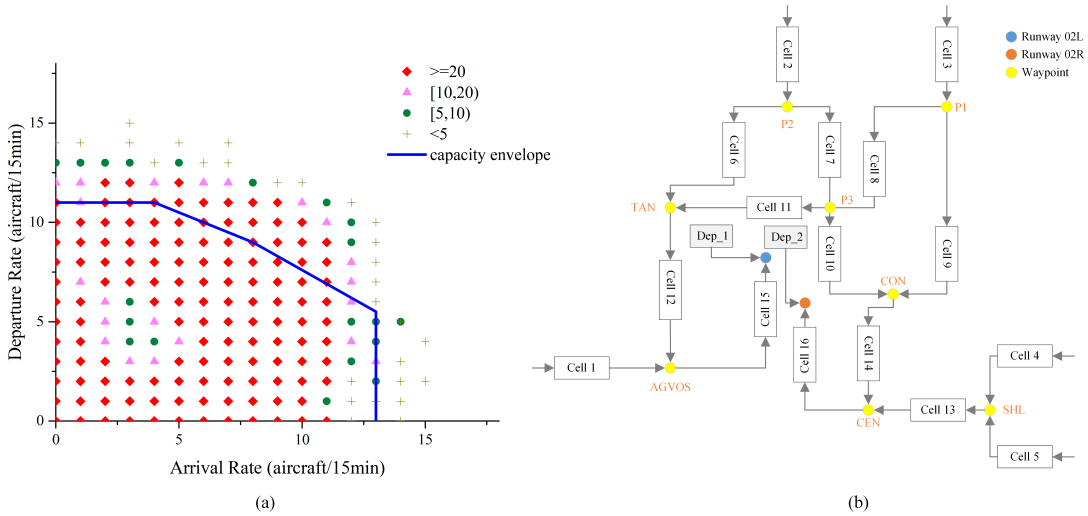

FIGURE 11. (a) Runway capacity envelope of Guangzhou airport. Different dots present the frequency of occurrence. (b) Cell network of arrival in in Guangzhou terminal airspace.

TABLE 2. Settings of cell level parameters.

	cell1	cell2	cell3	cell4	cell5	cell6	cell7	cell8	cell9	cell10	cell11	cell12	cell13	cell14	cell15	cell16
v_i(km/h)	620	620	620	620	620	580	580	580	580	580	580	580	500	500	350	350
v_i^0(km/h)	420	500	500	500	500	450	450	450	450	450	450	420	350	350	250	250
l_i(km)	112	36	45	55	45	105	50	55	76	33	70	112	83	96	55	55
d_i(km)	20	20	20	20	20	20	20	20	20	20	20	20	16	16	12	12
w_i(km/h)	83	83	83	83	83	78	78	78	78	78	78	78	89	89	78	78

then the sequence of entering into cell 3 is $[f_1, f_2, f_7, f_3, f_4, f_8]$ since $p_1/p_2 = 2$.

(2) Diverge cells. Turning ratio which is the crucial factor is determined by demand of the upstream cell. As shown in Figure10 (b), $D_4(t) = 4$, and turning ratios are derived by route information denoted by $\alpha_{4\to5}(t) = \alpha_{4\to6}(t) = 0.5$. However, due to downstream congestion, outflows are limited to $y_{4\to5}(t) = y_{4\to6}(t) = 1$. Based on FIFO hypothesis, f_3 is not allowed to overtake f_2 and has to hold in cell 4. Short-cut behavior initiated by controllers to guide the aircraft direct to downstream route segment is not considered here.

B. CALIBRATION AND VALIDATION OF Q-MCTM FOR ARRIVAL FLOW IN TERMINAL AIRSPACE

1) CALIBRATION OF RUNWAY CAPACITY ENVELOPE

We first calibrate the capacity of the runway cell, which serves as a sink for flows in both final approach and departure queue, and is characterized by the trade-off between arrivals and departures as shown in Figure8. Take-off and landing data at Guangzhou airport were collected from July 2015 to December 2015, and plotted in Figure 11(a) to show the joint frequency distribution of the pairs of rates. A F-QR method is adopted to generate the envelope shown as the blue curve in Figure 11 (a).

2) CALIBRATION OF CRITICAL PARAMETERS

Based on empirical data and fundamental diagram in Figure 5, required by MCTM and simulation, we construct the cell network (as shown in Figure11 (b)) of arrival routes in terminal airspace of ZGGG, which has two parallel runways that are operated with dependent arrivals but independent departures. A series of critical cell-level parameters like free flow speed, lowest speed, controlled separation, minimum separation in each cell are calibrated in Table2 according to local operations rules and empirical data. Besides, maximum length of each runway queuing here is set as 5 aircraft according to the operational regulations.

Terminal airspace operation on 11/09/2015 is simulated as the baseline. Accuracy metric is defined as the gap between simulated and empirical LR per 15 minutes; the efficiency metric is the computational time of simulation implemented in Matlab 2012 on a standard PC with 4.0 GB of RAM and an Intel Core i5 2410M processor running at 2.43 GHz. The relationship between simulation error and computing time is

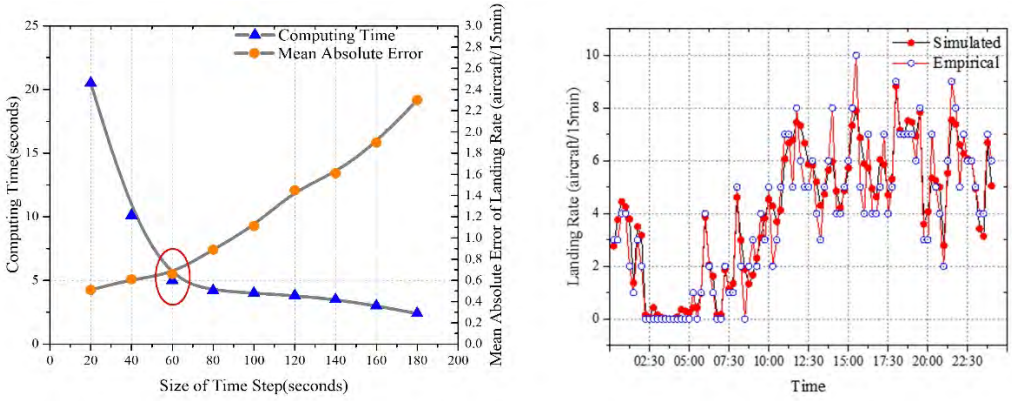

FIGURE 12. The selection of time step for simulation. (a) Trade-off between simulation accuracy and computational efficiency. (b) Comparison between empirical and simulated landing rate.

TABLE 3. The accuracy comparison of MCTM with and without QI.

Q-MCTM				MCTM			
Abs. Error		Rel. Error		Abs. Error		Rel. Error	
Mean	Std.	Mean	Std.	Mean	Std.	Mean	Std.
Arrival demand in cell6-cell9(aircraft)							
0.49	0.33	5.9%	4.8%	1.22	0.73	15.1%	9.3%
Landing Rate of runway 02L(aircraft/15min)							
0.30	0.28	3.5%	3.4%	0.82	0.59	9.5%	5.6%
Landing Rate of runway 02R(aircraft/15min)							
0.37	0.31	4.4%	4.1%	0.78	0.48	9.3%	6.4%

shown in Figure 12(a). One minute is chosen as the size of time step for the best balance between model accuracy and computational efficiency.

3) VALIDATION OF Q-MCTM

Before validating the proposed Q-MCTM simulation, we firstly would like to justify the advantage of introducing queuing model into the MCTM. As aforementioned, the main function of QI is to determine the turning ratio by tracking and updating traffic in the cells, which is crucial to duplicate the spatial distribution of air traffic flow in real-world operations as much as possible. However, MCTM simulator is able to run without QI by setting a fixed turning ratio for each time window according to the radar data or flight plan roughly, where the length of time window can be determined by the travel time using free flow speed in the cell. Here, we collect the empirical and simulated arrival demand in diverge cells (i.e., cell6-cell9 in Figure 11(b)) every one minute and landing rate every 15min, respectively, the accuracy of MCTM simulation with and without QI is summarized in Table 3. As you can see clearly, the adoption of queue model brings significant improvement of accuracy in simulating arrival demand in diverging cells that present fast time-vary turning ratios, which further leads to noticeable decrease of error for the landing rate on each runway. In the following, the validation only for Q-MCTM will be elaborated.

The Q-MCTM-based arrival network simulation is validated on two different levels.

On individual cell level, the proposed MCTM is capable of capturing phase transitions from free to congestion. Figure 13 shows the density-flow and density-speed evolution of both simulated and empirical traffic along merged links GYA-AGVOS (cell 1) and TAN-AGVOS (cell 12) as examples. Apparently, the maximum flow rate and speed for the same density in simulation is lower than that in empirical data. That is simply because we use piecewise fit to construct approximated fundamental diagrams for CTM based on empirical data as shown in Figure 3(a) and (b). In general, the average deviation of the absolute and relative errors throughout all cells are summarized in Table 4. The results show that the proposed simulation captures the cell dynamics with acceptable accuracy (absolute mean error of cell-based flow is less than 0.3aircraft/5min with standard deviation of about 0.15aircraft/5min). To be more specific, Figure 14 shows that cells which are closer to the runways perform higher simulation accuracy measured by both absolute and relative errors. The main reason is interpreted as the "Speed Convergence Effect". It means the speed differences among flights along route segments that closer to the runways are less significant due to standard flight procedure regulations and more constraints caused by higher traffic density. Especially for cell 15 and 16, runway capacity envelope plays an additional vital constraint for outflow rate and contributes to the best performance of cell-level accuracy.

Overall, it should be noted that, although the mean error is quite small, the standard deviation is relatively high. Same feature of simulation error is also observed on network level,

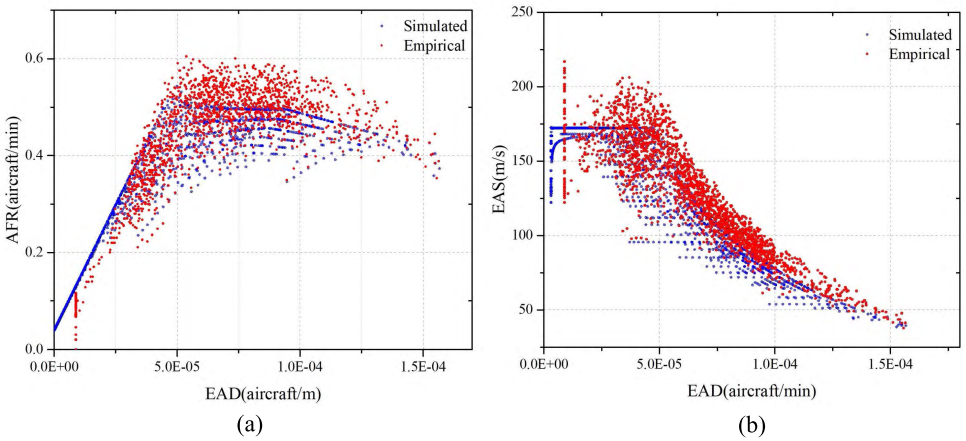

FIGURE 13. Comparison between empirical and simulated fundamental diagram. (a) Comparison between empirical and simulated EAD-AFR relation; (b) Comparison between empirical and simulated EAD-EAS relation.

TABLE 4. Average cell-based simulation error.

Cell-based Flow (aircraft/min)				Cell-based Speed (m/s)			
Abs. Error		Rel. Error		Abs. Error		Rel. Error	
Mean	Std.	Mean	Std.	Mean	Std.	Mean	Std.
0.052	0.037	9.23%	7.72%	13.2	8.08	9.33%	7.87%

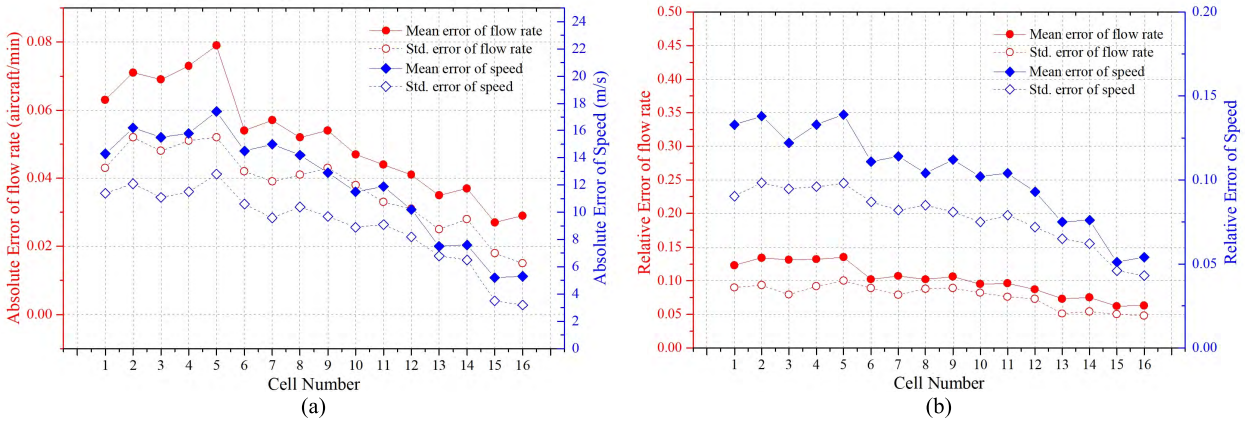

FIGURE 14. Simulation error of individual cell. (a) Absolute error of cells; (b) Relative error of cells.

which will be detailed in the following paragraph. These could be explained by significant fluctuation around the mean of empirical AFR and EAS for the same EAD (see scattered red dots in less congested phase in Figure 13 as an example) with average relative standard deviation of 17.6% and 16.1%, due to the heterogeneity of entry speed and flight performance of arriving aircraft.

On network level, one of the most important variables is the LR which presents the arrival network throughput efficiency of terminal airspace. As a sample demonstrated in Figure12(b), proposed MCTM simulation is validated and proved its reasonable high performance on arrival rate prediction for one-minute simulation time window. The absolute errors have a mean of 0.67 aircraft/15min and standard deviation of 0.55 aircraft/15min; the relative errors have a mean of 7.9% and standard deviation of 7.2%. Another

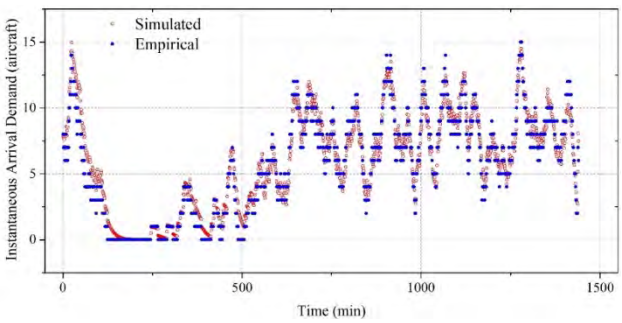

FIGURE 15. Comparison between empirical and simulated arrival demand in terminal airspace on 11/09/2015.

important variable is the AD which is a direct indicator of network congestion in terminal airspace defined in Section II. Figure 15 shows the empirical and simulated arrival demand

TABLE 5. The simulation error of LR and AD on network level.

LR (aircraft/15min)				AD (aircraft)			
Abs. Error		Rel. Error		Abs. Error		Rel. Error	
Mean	Std.	Mean	Std.	Mean	Std.	Mean	Std.
0.67	0.55	7.9%	7.2%	0.87	0.74	8.9%	9.2%

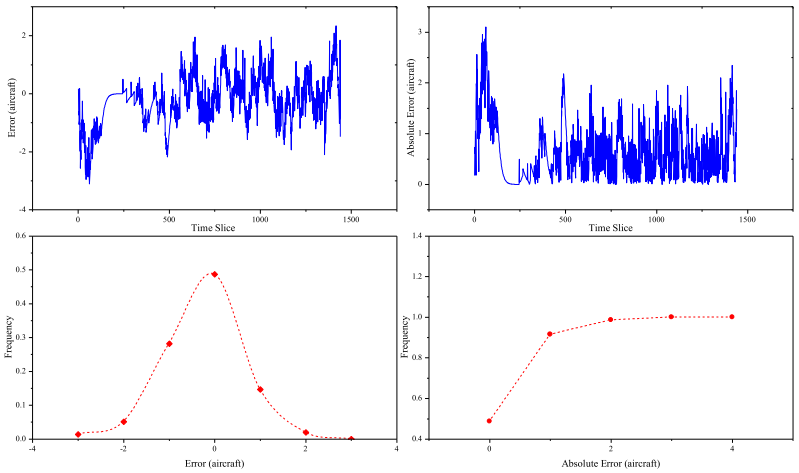

FIGURE 16. Simulation error of arrival demand on 11/09/2015.

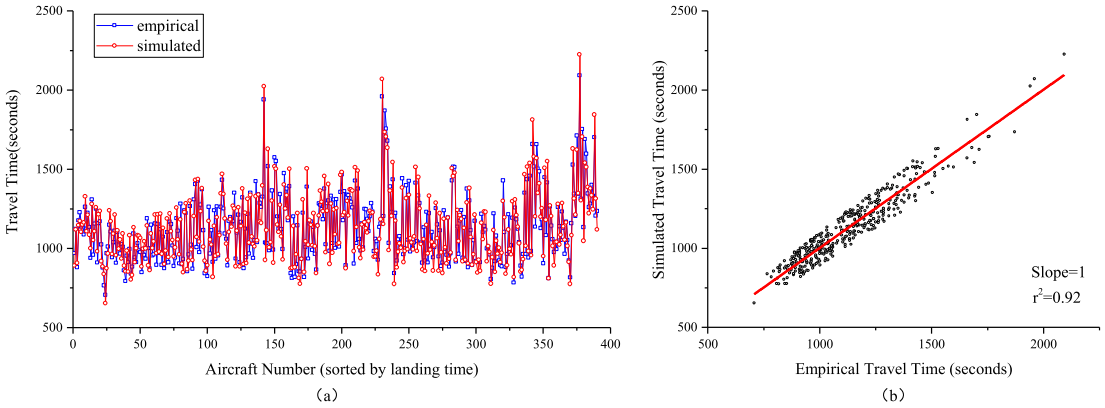

FIGURE 17. Comparison between simulated and empirical travel time. (a) Simulated and empirical travel time of each aircraft shown successively in accordance with landing sequence; (b) Proving the simulation accuracy by fitting the scatters using a line with slope of one (each dot presents the simulated and empirical travel time of a certain aircraft).

at the end of each minute as an example. The absolute errors have a mean of 0.87 aircraft and standard deviation of 0.74 aircraft; the relative errors have a mean of 8.9% and standard deviation of 9.2%. The detailed features of error are illustrated in Table 5 and Figure16.

Moreover, travel time is also a crucial parameter to validate the accuracy of simulation at network level. The travel time of each aircraft that determined by travel length and speed assigned by air traffic controllers, is a direct metric presenting its experiences of being manipulated in specific traffic situation during approach. Figure17 (a) shows the relationship between empirical and simulated travel time for each aircraft with the help of Queue Inspector. The absolute errors have a mean of 52s and standard deviation of 33.8s; the relative errors have a mean of 6.9% and standard deviation of 5.5%. By fitting the scatters which present the empirical and simulated travel time of each aircraft with the line y=x, the Pearson's r is 0.95, and $r^2 = 0.92$, as shown in Figure 17(b). The accuracy of the simulated travel time of arrival flight reasonably proves the effectiveness of the proposed MCTM model and hybrid simulation.

In addition, MFD-A characterized as aggregated "demand-supply" dynamics at network level is further validated. The absolute errors have a mean of 0.56 aircraft/15min and standard deviation of 0.51 aircraft/15min; the relative errors have a mean of 8.2% and standard deviation of 8.9%. Based on the network-wide simulation, we are able to construct the MFD-A, which is expressed as a

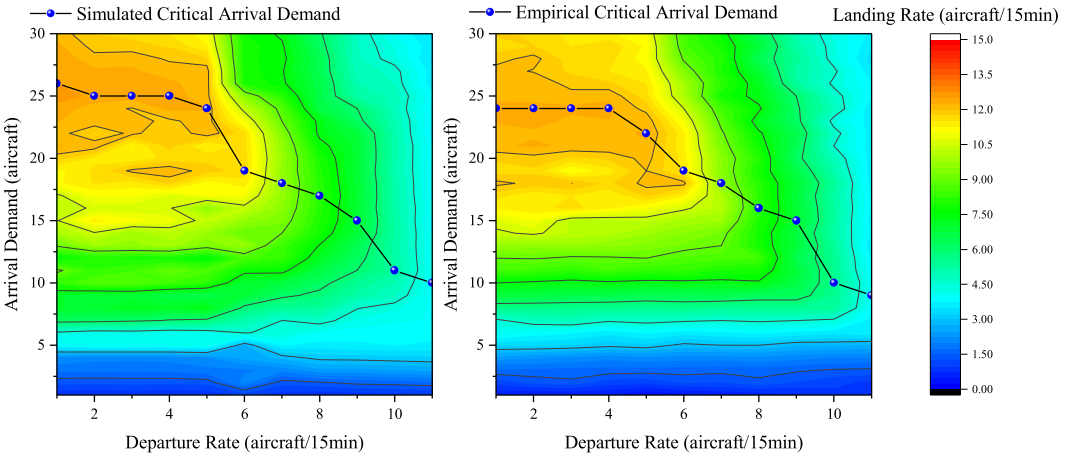

FIGURE 18. Comparison between simulated and empirical MFD-A.

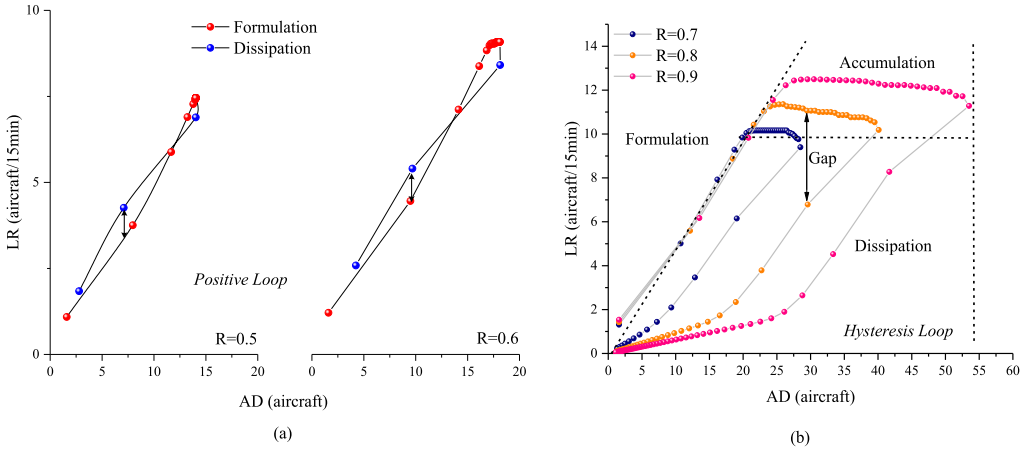

FIGURE 19. Full picture of MFD-A under various inflow rate.

function of both arrival demand and departure rate; see Figure 18. In this figure, the simulated MFD-A is compared with the empirical MFD-A. It can be seen that the CTM-based network simulation reasonably captures the nonlinear congestion effect and critical arrival demand in arrival network.

V. MACROSCOPIC CHARACTERISTICS ANALYSIS OF ARRIVAL FLOW DYNAMICS

A. FULL PICTURE OF CONGESTION EVOLUTION

Empirical and simulated MFD-A shows the general pattern of aggregate arrival flow dynamics from free to congestion. To further explore the comprehensive congestion evolution, an 8-hour arrival-only traffic scenario with increasing inflow rates R from 0.5 to 0.9 (aircraft/15min) is generated using the same operational parameter environment in Section IV.B. Figure 19 demonstrates different pictures of congestion development which consists of three phases named *formulation*, *accumulation* and *dissipation*.

Case1(R$<=$ 0.6): Congestion is not formulated, not to mention the accumulation phase. The arrival network supply and runway capacity is sufficient to handle with the arrival demand and to avoid the continuous growth of queuing length. Interestingly, during ''dissipation phase'' as shown by the blue dots in Figure 19(a), aircraft stop entering, and the *LR* is close to that in ''formulation phase'' or even larger when *AD* is less than 13 aircraft. For the absence of congestion, no spread effect is observed.

Case2 ($0.7 <= R < = 0.9$): Arrival flow with higher inflow rate achieves larger corresponding maximum *LR* with a similar increase rate. The ultimate *LR* of 12.5 aircraft/15min reaches at some critical *AD*around 26 when $R = 0.9$. This is an interesting finding that only when arrival rate climbs to its critical value at formulation phase, the ultimate *LR* corresponding with departure rate will be achieved. In addition, as the growth of inflow rate, the level of congestion accumulation gets more intensive presented by the expansion of maximum *AD* from 28 to 54. Moreover, compared to the *LR* in case1, severer congestion in case 2 leads to lower

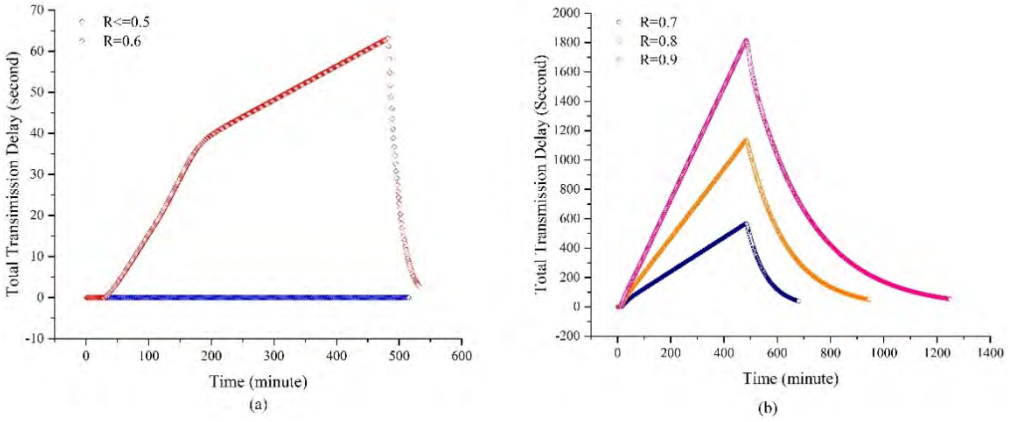

FIGURE 20. Delay evolves with time for various inflow rates.

efficiency of flow operation in dissipation phase shown by the ''Gap'' in Figure 19 (b).

In view of above analysis, different configurations of loops are presented in MFD-A in Figure 19. Here, we define ''positive loop'' for Case 1 and ''hysteresis loops'' for Case 2 for distinguishing. Spatial imbalance of traffic, congestion evolution and non-increasing speed profile of arrival aircraft could be the potential reasons for the existence of the loops.

- ''Positive Loops''. As the incoming of arrival flows, the density starts growing from 0 in terminal airspace, and the flights begin transmitting from arrival fixes to the runways. Obviously, in this period, the density in upstream sectors is significant higher than that in downstream ones near runway. The traffic density reaches steady and gets more uniform across all sectors as the arrivals keep flowing in formulation phase. At some moment, if we stop the inflow, arrivals turn to ''dissipation phase''. In this period, density in upstream sectors are getting lower and lower comparing to that near runways. Therefore, higher landing rates for the same arrival demand in ''dissipation phase'' are achieved, which develops a ''Positive Loop''.
- ''Hysteresis Loops''. Such ''hysteresis loops'' formed by formulation, accumulation and dissipation present some similar phenomenon which also can be observed in urban traffic congestion characterized by Generalized MFDs [48], [49]. In terminal airspace, congestion propagation and non-increasing speed profile of arrival aircraft could be the potential reason for existence of the ''loop''. As the spread of the flow, the spatial distribution of aircraft gets uniform across the airspace while the landing rate approach to the maximum in formulation phase. However, congestion starts accumulating when arrival demand goes beyond its critical value, and continue propagating back to the upstream where congestion gets severer, which leads to the decrease of EAS along flight routes and runway landing rate. In dissipation phase, traffic density in upstream is higher (i.e. holding strategies in real operation) than that near runway system. In such case, due to non-increasing speed features of arrival aircraft, the outflows discharge from severely congested upstream sectors are insufficient to fill available landing slots. Therefore, for the same level of arrival demand, the EAS and landing rate is significantly lower than that during formulation phase. The existence of ''hysteresis loop'' not only presents the weak efficiency of network in dissipation phase, but also provide a new perspective on predicting and evaluating the network congestion situation.

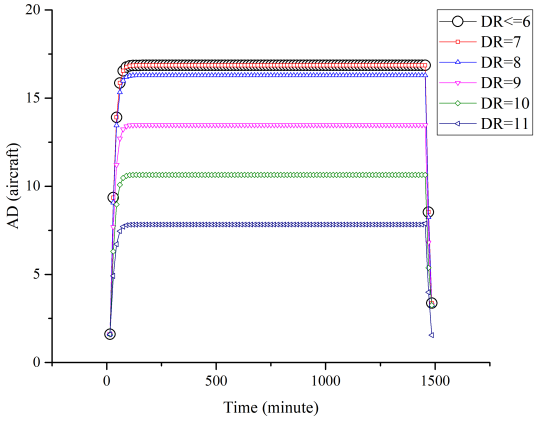

FIGURE 21. Arrival Demand (AD) changes in time at critical steady state for various departure rate.

Congestion propagation can be characterized by ''domino effect''-like flight delay, which provides another perspective on explaining the differences of the MFDs' in various inflow rate. To measure the level of flow congestion, a Total Transmission Delay (TTD) of cells during time step t is modeled as follows:

$$\Psi(t) = \sum_{i=1}^{U} \left(1 - \frac{v_i(t)}{v_i}\right) \cdot \Delta t \cdot \rho_i(t) \cdot l_i \tag{16}$$

where U is the number of cells.

TABLE 6. Key parameters of CSS in different departure situations.

Departure Rate (aircraft/15min)	0	1	2	3	4	5	6	7	8	9	10	11
CSI Rate (aircraft/min)	0.60	0.60	0.60	0.60	0.60	0.60	0.60	0.60	0.58	0.50	0.40	0.26
Landing Rate (aircraft/15min)	8.95	8.95	8.95	8.95	8.95	8.95	8.95	8.95	8.75	7.55	6.00	4.15
Capacity Usage (%)	71.6%	71.6%	71.6%	71.6%	71.6%	71.6%	76.2%	89.5%	100%	100%	100%	100%
Steady Arrival Demand (aircraft)	17	17	17	17	17	17	17	17	16	14	11	8

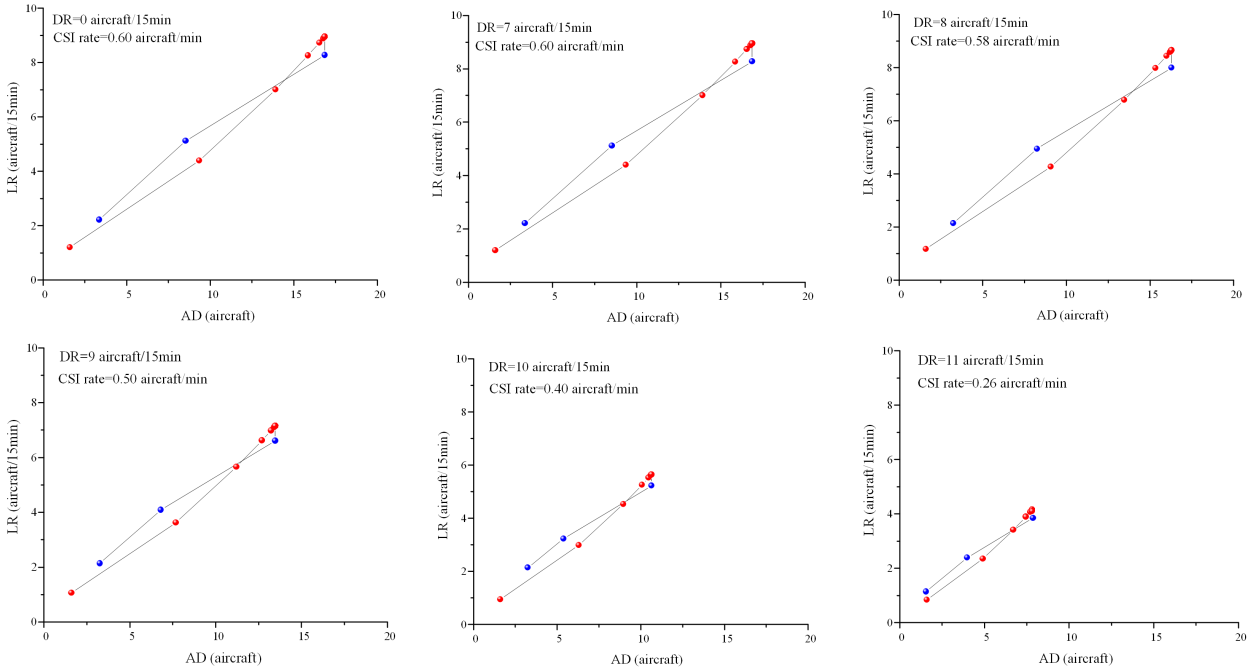

FIGURE 22. MFD-As at critical steady state for various departure rate.

Figure 20 shows the TTDs in cell network during each time window for different inflow rates. In Case1, arrival flow is transmitted through cell network smoothly with very slight and tolerable delay. Due to the high flow performance (shown in Figure20 (a)) in dissipation phase, very brief time is needed in this phase for the absence of congestion accumulation. However, as the increase of inflow rate, TTD and dissipation time grows significantly and become unacceptable as shown in Figure20 (b). This is why the number of dots in Figure20 becomes more in the scenarios with larger inflow rate.

A complete MFD-A in arrival network is a continuous and non-single valued function of occupancy (arrival demand) and throughput (landing rate) including formulation, accumulation and dissipation (or hysteresis) phases. However, the emergence of accumulation and hysteresis phenomenon in dissipation highly depends on the inflow rate. It is noted that, the same evolution patterns are observed (not detailed for simplification) for various departure demand. The main difference is the critical inflow rate that generates accumulation or hysteresis phases. So, Based on the above analysis of MFD-A and delay features, two critical states representing

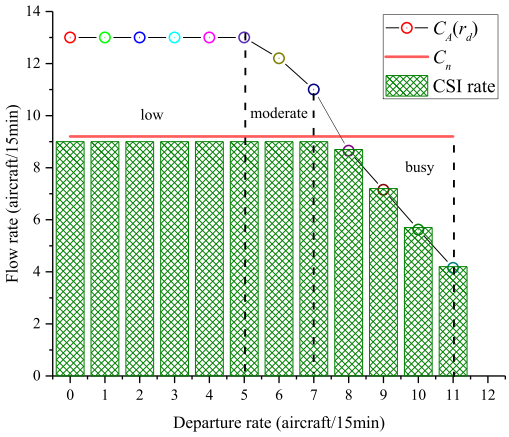

FIGURE 23. The relations between $C_A(r_d)$, C_n and CSI rate for different departure rate.

arrival flow dynamics are defined and discussed in following sections.

Definition 1 (Critical Steady State): There exists a maximum inflow rate that generates stabilized arrival demand in terminal airspace without accumulation. This traffic situation

TABLE 7. Key parameters of CUI in different departure situations.

Departure Rate (aircraft/15min)	0	1	2	3	4	5	6	7	8	9	10	11
CUI Rate (aircraft/min)	0.90	0.90	0.90	0.90	0.90	0.90	0.82	0.69	0.60	0.50	0.40	0.30
Acceptable duration (min)	90	90	90	90	90	90	120	300	540	640	700	790
Maximum Arrival Demand (aircraft)	30	30	30	30	30	30	27	25	27	25	20	16

is named as Critical Steady State (*CSS*) while the inflow is called Critical Stable Inflow (*CSI*)

Definition 2 (Critical Unsteady State): There exists a minimum inflow rate that generates full utilization of runway capacity. This traffic situation is named as Critical Unsteady State (*CUS*) while the inflow is called Critical Unstable Inflow (*CUI*).

B. CRITICAL STEADY STATE

In system theory, steady state is achieved as the behavior of the system or the process staying unchanged over time. In terminal air traffic management domain, as defined in *Definition 1*, CSS provides a crucial reference for optimal arrival flow control to minimize flight delay while making better use of system capacity.

Based on the same parameter environment of simulation used in Section IV.B, we search for the Critical Steady States by injecting continuous inflows under various departure rates from 0 to 11aircraft/15min. Figure 21 and Figure 22 verify the existence of *CSS* by presenting steady arrival demand without accumulation and MFD-A configurations, respectively.

To be numerically detailed, Table 6 shows some key flow characteristics at *CSS*. At *CSS*, inflow rate equals to the landing rate without any delay. By inspecting the trend of inflow rate together with landing rate, we find that as the raise of departure rate, the landing capacity usage increases

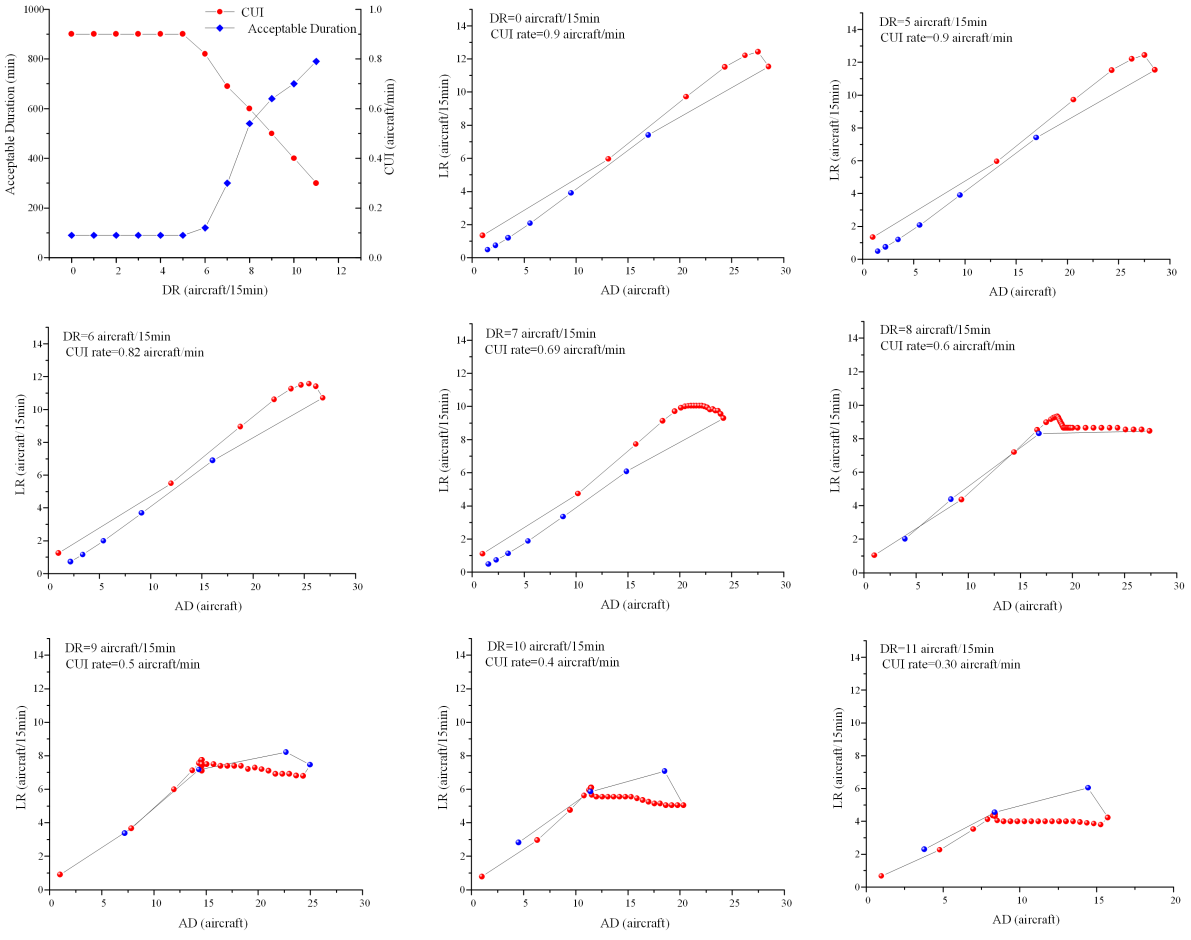

FIGURE 24. MFD-A at critical unsteady state under tolerable delay for various departure rate.

after 5 departures per 15 minutes while the landing rate keeps constant before 8 departures per 15 minutes. This interesting asynchronism results from the imbalance between landing capacity on runway denoted as $C_A(r_d)$ (i.e., a function of departure rate r_d) and maximum arrival network throughput at formulation phase denoted by C_n.

To be more specific, we explain the reason by dividing the departure rate into three category: low (0-5), moderate (6-7) and busy (8-11), as shown in Figure 23. At low departure level, the rate of *CSI* is constrained by C_n which is less than $C_A(r_d)$ as shown by the capacity usage. In moderate level, although landing capacity begins to drop, it is still above C_n. As a result, the inflow rate and landing rate stay still while capacity usage significantly increases. At busy level, $C_A(r_d)$ falls below C_n and becomes the key limitation of *CSI*rate. So, we can give a conclusion that the rate of *CSI* is determined by the bottleneck of the system as $R = \min\{C_A(r_d), C_n\}$.

C. CRITICAL UNSTABLE STATES

Increasing inflow rate dis-equilibrates the *CSS* as the accumulation of arrival demand and delay propagation. However, especially at busy or hub airports, peak-hour traffic is inevitable due to marketing demand, even requiring full utilization of runway capacity. To measure and understand the characteristics of arrival flow dynamics during peak-hour, we discuss the Critical Unstable Inflow for different departure rates and its acceptable duration based on tolerable average landing delay.

By inheriting the parameter environment used in Section IV.B, we search for the *CUI* and its acceptable duration in various departure rates from 0 to 11aircraft/15min. By investigating the maximum average landing delay experienced in Guangzhou terminal airspace, the tolerable average landing delay here is set as 5 minutes. Table 7 shows the characteristics of *CUS* in different departure scenarios. In general, ultimate landing rates are achieved in *CUS* generated by certain inflow rate which is just larger than that in *CSS*. As more departures require for take-off on the runways, the acceptable duration of *CUS* increases while the maximum arrival demand decreases. To be more detailed, as shown by MFD-A in Figure 24, the phase transitions from formulation to accumulation is getting slower in less busy departure scenarios and lead to longer duration but lower level of accumulation. In dissipation phase, hysteresis phenomenon emerges only if DR is less than 8 aircraft/15min.

The results suggest that during peak hour of departure, *CUS* can be maintained for a longer period to achieve full utilization of runway capacity without falling into severer congestion. However, the number of departures and arrivals at airport are approximately equal and dependent in a whole day. Any arrival flight will require for take-off on the runway after some certain turn-around time. In other words, once the turn-around time is known, the full profile of runway throughput rate is determined as long as arrival schedule is fixed. It is well recognized that refined flight wave (also known as arrival-departure schedule) has remarkable lifting effect on airport operation. Here, the features of *CUS* and its acceptable duration provide vital references for strategic airport flight schedule planning and pre-tactical air traffic flow optimization, especially for high density airports which normally operate at or around its runway capacity.

VI. CONCLUSIONS

The study of complex air traffic dynamics is essential for understanding the nature of air traffic flow and uncovering technical potentials for advancing air traffic management. Among a variety of analytical approaches, CTM-based network flow modeling is an effective and intuitive way to understand flow propagation at acceptable granularities. In order to explore arrival traffic flow dynamics in mesoscopic and macroscopic levels, empirical FD and MFD-A are established to provide initial understanding of flow dynamics using trajectory radar data of Guangzhou terminal airspace. Based on the empirical studies, a modified cell transmission model is developed with a novel introduction of Queuing Inspector for refining the simulation of the spatio-temporal propagation of flow and congestion in terminal airspace, and is shown to be an efficient and accurate simulator capable of supporting a wide range of applications such as arrival flow control, route planning and runway slot scheduling.

Using proposed simulation, we further reveal the full evolution process of MFD-A as a continuous and non-single valued function of occupancy (arrival demand) and throughput (landing rate) including formulation, accumulation and dissipation (or hysteresis) phases. Characteristics of macroscopic arrival flow dynamics in crucial states like Critical Steady States and Critical Unsteady States detailed discussed provide strategy potentials for ATFM.

This paper is an adapted and follow-up study of the fundamental relationship between ''occupancy'' and ''throughput'' on mesoscopic and macroscopic levels for air traffic flow in terminal airspace, which manifest themselves as the link-based FD and network-based MFD, respectively. Both empirical evidence and analytical models are employed to verify these notions and develop efficient network simulation that hold promise in supporting further air traffic management initiatives. As a future study, it is essential to extend the modeling to integrated arrival and departure traffic, although departure traffic normally perform smooth status after take-off. Therefore, air-ground integrated modeling of airport surface and surrounding airspace [64]–[65] based on refined fundamental diagram appears to be more significant in characterizing the integral dynamics and to underpinning the implementation the advanced airport-terminal operational concepts and automation integration.

APPENDIX A. CAPACITY OF WAYPOINT

A point-capacity constraint (indicated as M in Figure 6) denoted by C_M subject to separation minimum, speed, and especially the geometry features at the junctions (merge/diverge/crossover) even at simple connections.

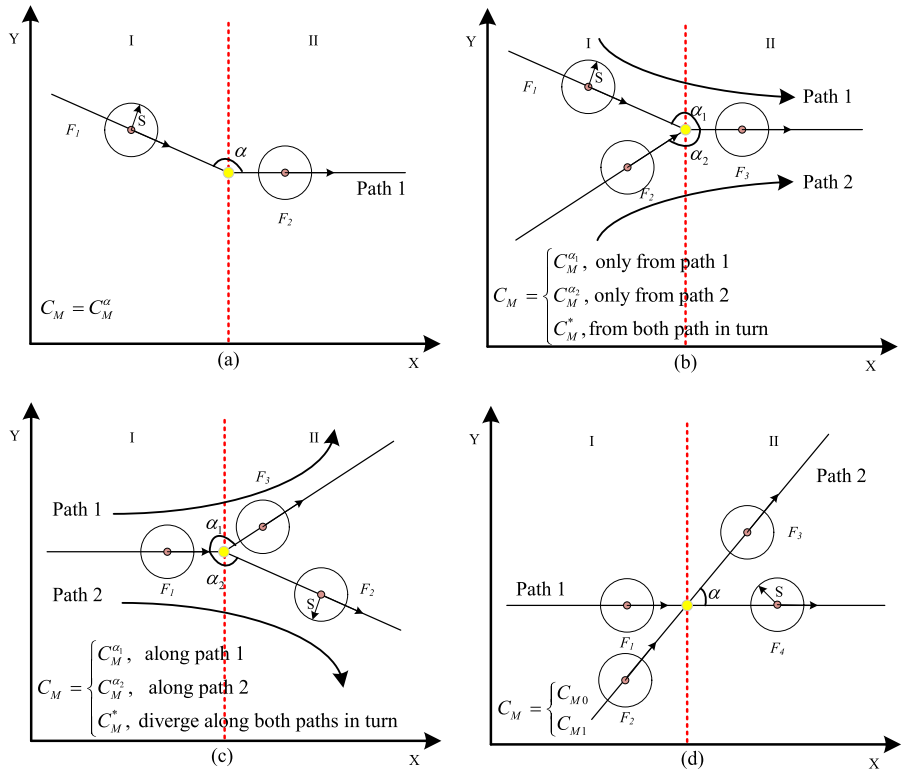

FIGURE 25. Schema of point capacity at different junctions. (a) simple connection; (b) merge connection; (c) diverge connection; (d) crossover connection.

As shown in Figure25, conflict-free should be guaranteed within and between Area I and II. Here, we take merge scenario as an example for the sake of simplification shown in Figure 25(b).

We make the following observation: (a) if two or more consecutive aircraft advance through junction only along path 1 or path 2, the capacity of the junction is denoted as $C_M^{\alpha_1}$ and $C_M^{\alpha_2}$, respectively; (b) if two upstream approaches take turn to discharge aircraft, the capacity is denoted as C_M^*, which is detailed below.

Without loss of generality, it is assumed that aircraft a and b are flying in Area I along different paths with speed v_a and v_b, respectively (see Figure 26). Aircraft a passes point M at $t = 0$ beforehand, and adjusts its speed to $v_{a,i}$ after entering route i. At this moment, the horizontal separation between the aircraft pair is noted by L. Therefore, the function of horizontal distance changes with time can be formulated as:

$$x^2 = F(t) = \left(v_b^2 + v_{a,i}^2 + 2v_{a,i}v_b cos\alpha_1\right) t^2 - 2L\left(v_b + v_{a,i}cos\alpha_1\right) t + L^2 \quad (17)$$

which is a quadratic function of independent variable t. Its second derivative $F''(t) = v_b^2 + v_{a,i}^2 + 2v_{a,i}v_b cos\alpha_1 > 0$ proves x^2 achieves its minimum at $F'(t) = 0$, when

$$t_0 = \frac{L\left(v_b + v_{a,i}cos\alpha_1\right)}{v_b^2 + v_{a,i}^2 + 2v_{a,i}v_b cos\alpha_1} \quad (18)$$

Case 1: If $t_0 > 0$, the minimum distance x_0 between the aircraft pair will be observed in Area II.

$$x_0 = L\frac{v_{a,i}sin\alpha_1}{\sqrt{v_b^2 + v_{a,i}^2 + 2v_{a,i}v_b cos\alpha_1}} \geq S \quad (19)$$

where S is the minimum horizontal separation in terminal airspace.

The critical distance L_0 between aircraft a and b at $t = 0$ can be derived when we let $S = x_0$.

$$L_0 = S\frac{\sqrt{v_b^2 + v_{a,i}^2 + 2v_{a,i}v_b cos\alpha_1}}{v_{a,i}sin\alpha_1} \quad (20)$$

Therefore, the capacity of point M in this case is denoted as $C_M^{*1} = v_b/L_0$

Case 2: If $t_0 \leq 0$, the minimum distance x_0 between the aircraft pair may be observed in Area I. In this situation, the horizontal distance is Area I is formulated as

$$x = \sqrt{(v_a t)^2 + (L - v_b t)^2 + 2v_a t(L - v_b t)cos\beta} \quad (21)$$

Similarly, the moment when the horizontal distance between the aircraft pair reach its minimum in Area I is

$$t_0' = \frac{L(v_b - v_a cos\beta)}{v_b^2 + v_{a,i}^2 - 2v_{a,i}v_b cos\alpha_1} \quad (22)$$

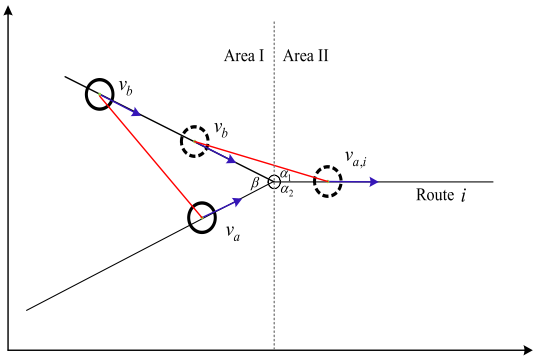

FIGURE 26. Schema of aircraft operation at merging point.

If $t_0^{'} > 0$, the minimum distance is observed at $t = 0$, i.e. $L = S$; or

$$L_1 = S\frac{\sqrt{v_b^2 + v_a^2 - 2v_a v_b cos\beta}}{v_a sin\alpha_1} \tag{23}$$

In all, the temporal distance between aircraft a and b when aircraft a passing converging point M beforehand is

$$T_M^{a,b} = \begin{cases} L_0/v_b, \\ \quad if\ v_b + v_{a,i}cos\alpha_1 > 0 \\ L_1/v_b, \\ \quad if\ v_b + v_{a,i}cos\alpha_1 < 0\ and\ v_b - v_a\ cos\beta < 0 \\ S/v_b, \\ \quad if\ v_b + v_{a,i}cos\alpha_1 < 0\ and\ v_b - v_a cos\beta > 0 \end{cases} \tag{24}$$

The temporal distance can be similarly derived when aircraft b passing merging point M beforehand, denoted as $T_M^{b,a}$. Therefore, the capacity of point M in flow pattern (b) is

$$C_M^* = \frac{1}{2}\left(C_M^{a,b} + C_M^{b,a}\right) = \frac{1}{2}\left(\frac{1}{T_M^{a,b}} + \frac{1}{T_M^{b,a}}\right) \tag{25}$$

As for pattern (a), if $t_0 > 0$, the critical distance at $t = 0$ can be derived based on the same method in Case 1; if $t_0 < 0$, then the critical distance when aircraft a passing merging point M is equal to S.

Similarly, the point capacity at different junctions can be always derived as the function of average flow speed and connecting angles. Obviously, as shown in Figure 25, point capacity at merge/diverge/crossover junction is dynamic subject to air traffic flow structure, and is an essential parameter in flow transmission modeling.

DECLARATION OF CONFLICTING INTERESTS

The authors declare that there is no conflict of interest regarding the publication of this paper.

REFERENCES

[1] E. G. Bowen and T. Pearcey, "Delays in the flow of air traffic," *Aeronaut. J.*, vol. 52, no. 448, pp. 251–258, 1948.
[2] A. L. David, C. Nelson, and G. Shapiro, "The aviation system analysis capability: Airport Capacity and Delay Models," NASA AMES Res. Center, Moffett Field, CA, USA, Tech. Rep. NASA/CR-1998-207659, Apr. 1998.
[3] B. S. Levy, "Track averages and traffic pattern characterization for airspace analysis," in *Proc. 22nd DASC*, Indianapolis, IN, USA, Oct. 2003, p. 1.E.4-11-10.
[4] A. Eckstein, "Automated flight track taxonomy for measuring benefits from performance based navigation," in *Proc. ICNSC*, Arlington, VA, USA, May 2009, pp. 1–12.
[5] M. Gariel, A. N. Srivastava, and E. Feron, "Trajectory clustering and an application to airspace monitoring," *IEEE Trans. Intell. Transp. Syst.*, vol. 12, no. 4, pp. 1511–1524, Dec. 2011.
[6] R. Annoni and C. H. Q. Forster, "Analysis of aircraft trajectories using Fourier descriptors and kernel density estimation," in *Proc. IEEE ICITS*, Anchorage, AK, USA, Sep. 2012, pp. 1441–1446.
[7] M. Enriquez, "Identifying temporally persistent flows in the terminal airspace via spectral clustering," presented at the 10th USA/Eur. ATM R&D Seminar, Chicago, IL, USA, 2013.
[8] Y. Xu, H. Zhang, Z. Liao, and L. Yang, "A dynamic air traffic model for analyzing relationship patterns of traffic flow parameters in terminal airspace," *Aerosp. Sci. Technol.*, vol. 55, pp. 10–23, Aug. 2016.
[9] B. Sridhar, K. Sheth, and S. Grabbe, "Airspace complexity and its application in air traffic management," presented at the 2nd USA/Eur. ATM R&D Seminar, Orlando, FL, USA, 1998.
[10] I. V. Laudeman, S. G. Shelden, and R. Branstrom, "Dynamic density: An air traffic management metric," NASA AMES Res. Center, Moffett Field, CA, USA, Tech. Rep. NASA/TM-1998-112226, Apr. 1998.
[11] M. Whiteley, "PHARE advanced tools tactical load smoother," Eur. Org. Saf. Air Navigat., Brussels, Belgium, Tech. Rep. 99-70-18, 1999.
[12] K. Lee, E. Feron, and A. Pritchett, "Describing airspace complexity: Airspace response to disturbance," *J. Guid., Control Dyn.*, vol. 32, no. 1, pp. 210–222, 2009.
[13] S. Puechmorel and D. Delahaye, "New trend in air traffic complexity," presented at the EIWAC, Tokyo, Japan, Mar. 2009.
[14] J. G. d'Engelbronner, C. Borst, J. Ellerbroek, M. M. van Paassen, and M. Mulder, "Solution-space–based analysis of dynamic air traffic controller workload," *J. Aircraft*, vol. 52, no. 4, pp. 1146–1160, 2015.
[15] R. M. Harris, "Models for runway capacity analysis," MITRE, Washington, DC, USA, Tech. Rep. MTR-4102, 1969.
[16] M. Janić and V. Tošić, "Terminal airspace capacity model," *Transp. Res. A, Gen.*, vol. 16, no. 4, pp. 253–260, 1982.
[17] M. Hansen, "Micro-level analysis of airport delay externalities using deterministic queuing models: A case study," *J. Air Transp. Manage.*, vol. 8, no. 2, pp. 73–87, 2002.
[18] P. K. Menon, M. Tandale, J. Kim, and P. Sengupta, "A Framework for Stochastic Air Traffic Flow Modeling and Analysis," presented at the AIAA Guid., Navigat., Control Conf., 2010.
[19] N. Pyrgiotis, K. M. Malone, and A. Odoni, "Modelling delay propagation within an airport network," *Transp. Res. C, Emerg. Technol.*, vol. 27, pp. 60–75, Feb. 2013.
[20] T. Ezaki and K. Nishinari, "Potential global jamming transition in aviation networks," *Phys. Rev. E, Stat. Phys. Plasmas Fluids Relat. Interdiscip. Top.*, vol. 90, no. 2, Aug. 2014, Art. no. 022807.
[21] A. M. Bayen, R. L. Raffard, and C. J. Tomlin, "Adjoint-based control of a new Eulerian network model of air Traffic Flow," *IEEE Trans. Control Syst. Technol.*, vol. 14, no. 5, pp. 804–818, Sep. 2006.
[22] M. J. Lighthill and J. B. Whitham, "On kinematic waves II. A theory of traffic flow on long crowded roads," *Proc. Roy. Soc.*, vol. 229, pp. 317–345, May 1955.
[23] C. F. Daganzo, "The cell transmission model: A dynamic representation of highway traffic consistent with the hydrodynamic theory," *Transp. Res. B, Methodol.*, vol. 28, no. 4, pp. 269–287, Aug. 1994.
[24] H. B. Celikoglu, "Dynamic classification of traffic flow patterns simulated by a switching multimode discrete cell transmission model," *IEEE Trans. Intell. Transp. Syst.*, vol. 15, no. 6, pp. 2539–2550, Dec. 2014.
[25] H. B. Celikoglu and M. A. Silgu, "Extension of traffic flow pattern dynamic classification by a macroscopic model using multivariate clustering," *Transp. Sci.*, vol. 50, no. 3, pp. 966–981, 2016.
[26] K. Tiaprasert, Y. Zhang, C. Aswakul, J. Jiao, and X. Ye, "Closed-form multiclass cell transmission model enhanced with overtaking, lane-changing, and first-in first-out properties," *Transp. Res. C, Emerg. Technol.*, vol. 85, pp. 86–110, Dec. 2017.
[27] T. L. Friesz, J. Luque, R. L. Tobin, and B. W. Wie, "Dynamic network traffic assignment considered as a continuous time optimal control problem," *Oper. Res.*, vol. 37, no. 6, pp. 893–901, 1989.

[28] H. B. Celikoglu, "A dynamic network loading process with explicit delay modelling," *Transp. Res. C, Emerg. Technol.*, vol. 15, no. 5, pp. 279–299, 2007.
[29] H. B. Celikoglu, E. Gedizlioglu, and M. Dell'Orco, "A node-based modeling approach for the continuous dynamic network loading problem," *IEEE Trans. Intell. Transp. Syst.*, vol. 10, no. 1, pp. 165–174, Mar. 2009.
[30] H. B. Celikoglu, "A dynamic network loading model for traffic dynamics modeling," *IEEE Trans. Intell. Transp. Syst.*, vol. 8, no. 4, pp. 575–583, Dec. 2007.
[31] P. K. Menon, G. D. Sweriduk, and K. Bilimoria, "New approach for modeling, analysis, and control of air traffic flow," *J. Guid., Control, Dyn.*, vol. 27, no. 5, pp. 737–744 2004.
[32] P. K. Menon, G. D. Sweriduk, and T. Lam, "Computer-aided Eulerian air traffic flow modeling and predictive control," *J. Guid., Control, Dyn.*, vol. 29, no. 1, pp. 12–19, 2006.
[33] D. Sun and A. M. Bayen, "Multicommodity Eulerian-Lagrangian large-capacity cell transmission model for en route traffic," *J. Guid., Control, Dyn.*, vol. 31, no. 3, pp. 616–628, 2008.
[34] P. Wei, Y. Cao, and D. Sun, "Total unimodularity and decomposition method for large-scale air traffic cell transmission model," *Transp. Res. B, Methodol.*, vol. 53, pp. 1–16, Jul. 2013.
[35] Y. Cao and D. Sun, "Link transmission model for air traffic flow management," *J. Guid., Control, Dyn.*, vol. 34, no. 5, pp. 1342–1351, 2011.
[36] H. Zhang, Y. Xu, L. Yang, and H. Liu, "Macroscopic model and simulation analysis of air traffic flow in airport terminal area," *Discrete Dyn. Nature Soc.*, vol. 2014, Aug. 2014, Art. no. 741654.
[37] L. Yang, S. Yin, K. Han, J. Haddad, and M. Hu, "Fundamental diagrams of airport surface traffic: Models and applications," *Transp. Res. B, Methodol.*, vol. 106, pp. 29–51, Dec. 2017.
[38] C. F. Daganzo, "Urban gridlock: Macroscopic modeling and mitigation approaches," *Transp. Res. B, Methodol.*, vol. 41, no. 1, pp. 49–62, 2007.
[39] N. Geroliminis and C. F. Daganzo, "Existence of urban-scale macroscopic fundamental diagrams: Some experimental findings," *Transp. Res. B, Methodol.*, vol. 42, no. 9, pp. 759–770, Nov. 2008.
[40] C. Buisson and C. Ladier, "Exploring the impact of homogeneity of traffic measurements on the existence of macroscopic fundamental diagrams," *Transp. Res. Rec. J. Transp. Res. Board*, vol. 2124, pp. 127–136, Dec. 2009.
[41] J. Haddad, M. Ramezani, and N. Geroliminis, "Cooperative traffic control of a mixed network with two urban regions and a freeway," *Transp. Res. B, Methodol.*, vol. 54, no. 8, pp. 17–36, Aug. 2013.
[42] N. Geroliminis, J. Haddad, and M. Ramezani, "Optimal perimeter control for two urban regions with macroscopic fundamental diagrams: A model predictive approach," *IEEE Trans. Intell. Transp. Syst.*, vol. 14, no. 1, pp. 348–359, Mar. 2013.
[43] M. Keyvan-Ekbatani, M. Papageorgiou, and I. Papamichail, "Urban congestion gating control based on reduced operational network fundamental diagrams," *Transp. Res. C, Emerg. Technol.*, vol. 33, pp. 74–87, Aug. 2013.
[44] M. Keyvan-Ekbatani, M. Papageorgiou, and V. L. Knoop, "Controller design for gating traffic control in presence of time-delay in urban road networks," *Transp. Res. C*, vol. 59, pp. 308–322, Jan. 2015.
[45] Raytheon ATMSDI Team, "Airspace concept evaluation system: Build 2 software user manual," Raytheon ATMSDI Team, NASA AMES Res. Center, Mountain View, CA, USA, Tech. Rep. CTOD7.29, 2003.
[46] K. D. Bilimaria, B. Sridhar, G. B. Chatterji, G. Sheth, and S. Grabbe, "FACET: Future ATM concepts evaluation tool," presented at the 3rd USA/Eur. Air Traffic Manage. Seminar, Naples, Italy, 2000.
[47] C. F. Daganzo, "The cell transmission model, part II: Network traffic," *Transp. Res. B, Methodol.*, vol. 29, no. 2, pp. 79–93, 1995.
[48] V. V. Gayah and C. F. Daganzo, "Clockwise hysteresis loops in the macroscopic fundamental diagram: An effect of network instability," *Transp. Res. B, Methodol.*, vol. 45, no. 4, pp. 643–655, 2011.
[49] V. L. Knoop, H. van Lint, and S. P. Hoogendoorn, "Traffic dynamics: Its impact on the Macroscopic Fundamental Diagram," *Phys. A, Stat. Mech. Appl.*, vol. 438, pp. 236–250, Nov. 2015.
[50] L. Yang, S. Yin, M. Hu, K. Han, and H. Zhang, "Empirical exploration of air traffic and human dynamics in terminal airspaces," *Transp. Res. C, Emerg. Technol.*, vol. 84, pp. 219–244, Nov. 2017.
[51] D. L. Gerlough, "Traffic flow theory," Transp. Res. Board, Nat. Res. Council, Washington, DC, USA, Tech. Rep. 165, 1975.
[52] J. M. Del Castillo and F. G. Benítez, "On the functional form of the speed-density relationship—II: Empirical investigation," *Transp. Res. B, Methodol.*, vol. 29, no. 5, pp. 391–406, 1995.
[53] E. P. Gilbo, "Airport capacity: Representation, estimation, optimization," *IEEE Trans. Control Syst. Technol.*, vol. 1, no. 3, pp. 144–154, Sep. 1993.
[54] R. Courant, K. Friedrichs, and H. Lewy, "Über die partiellen differenzengleichungen der mathematischen Physik," *Mathematische Annalen*, vol. 100, no. 1, pp. 32–74, 1928.
[55] W. L. Jin and H. M. Zhang, "On the distribution schemes for determining flows through a merge," *Transp. Res. B, Methodol.*, vol. 37, no. 6, pp. 521–540, 2003.
[56] M. Garavello, K. Han, and B. Piccoli, *Models for Vehicular Traffic on Networks* (AIMS Series on Applied Mathematics). Springfield, IL, USA, 2016.
[57] L. Yang, M.-H. Hu, S.-W. Yin, and Z. Zhao, "Statistical method of coupled peak service ability assessment for multi-airport system," *Aeronaut. Comput. Techn.*, vol. 5, pp. 1–4, Dec. 2015.
[58] F. van Wageningen-Kessels, H. Van Lint, K. Vuik, and S. Hoogendoorn, "Genealogy of traffic flow models," *EURO J. Transp. Logistics*, vol. 4, no. 4, pp. 445–473, 2015.
[59] M. Dell'Orco, "A dynamic network loading model for mesosimulation in transportation systems," *Eur. J. Oper. Res.*, vol. 175, no. 3, pp. 1447–1454, 2006.
[60] H. B. Celikoglu and M. Dell'Orco, "Mesoscopic simulation of a dynamic link loading process," *Transp. Res. C, Emerg. Technol.*, vol. 15, no. 5, pp. 329–344, 2007.
[61] M. Dell'Orco, M. Marinelli, and M. A. Silgu, "Bee colony optimization for innovative travel time estimation, based on a mesoscopic traffic assignment model," *Transp. Res. C, Emerg. Technol.*, vol. 66, pp. 48–60, 2016.
[62] C. Antoniou, H. B. Celikoglu, and N. Geroliminis, "Special issue on advanced network traffic management: From dynamic state estimation to traffic control," *Transp. Res. C, Emerg. Technol.*, vol. 66, pp. 48–60, May 2016.
[63] T. L. Friesz, K. Han, P. A. Neto, A. Meimand, and T. Yao, "Dynamic user equilibrium based on a hydrodynamic model," *Transp. Res. B, Methodol.*, vol. 47, pp. 102–126, Jan. 2013.
[64] J. Ma, D. Delahaye, M. Sbihi, P. Scala, and M. A. M. Mota, "Integrated optimization of terminal maneuvering area and airport at the macroscopic level," *Transp. Res. C, Emerg. Technol.*, vol. 98, pp. 338–357, Jan. 2019.
[65] D. Bertsimas and M. Frankovich, "Unified optimization of traffic flows through airports," *Transp. Sci.*, vol. 50, no. 1, pp. 77–93, 2016.

LEI YANG received the B.E. degree in air traffic management engineering and the M.E. and Ph.D. degrees in transportation planning and management from the Nanjing University of Aeronautics and Astronautics (NUAA), Nanjing, China, in 2009, 2012, and 2018, respectively. From 2016 to 2018, he was a joint training Ph.D. student with the Faulty of Aerospace Engineering, TU Delft, The Netherlands. Since 2018, he has been an Assistant Professor with NUAA. He has published more than 20 high-level journals and conference papers, including ATM Seminar, *Transportation Research Part B and C*. His research interests include complex air traffic system modeling, new type airspace design and operation, trajectory-based air traffic management (ATM), and intelligent air traffic control solutions. He has participated in several national scientific projects, including the National High-tech R&D Program of China and the National Natural Science Foundation of China. He is also active in ATM-related academic activities as a reviewer and a session co-chair.

SUWAN YIN received the B.E. and M.E. degrees in transportation planning and management from the Nanjing University of Aeronautics and Astronautics, in 2011 and 2015, respectively. She is currently a Ph.D. Researcher with the Center for Transport Studies, Imperial College London. After receiving the M.E. degree from the National Key Laboratory of ATFM, she worked there as a Research Associate before moving to Imperial College as a Ph.D. Researcher, where she participated in more than 20 industrial projects and academic research in terms of the airport surface and airport terminal operation and optimization. She has published 18 journals (i.e., *Transportation Research Part B and C*) and conference papers (i.e., AIAA and TRB) and presented her research on the international conference for three times. Her research interests include airport surface optimization, airport terminal optimization, transportation network modeling, traffic control and management, and sustainable transportation. She is also a Researcher of Cloud-Guizhou Big Data Science & Application Research Center, and a committee member of the Chinese Overseas Transportation Association (COTA) and the Transportation Research Board (TRB).

MINGHUA HU was born in Hunan, China, in 1962. He received the B.M. degree in electrical automation and the M.E. degree in aircraft navigation and control from the Nanjing University of Aeronautics and Astronautics (NUAA), in 1982 and 1987, respectively, where he is currently a Professor and a Doctoral Supervisor with the Civil Aviation College. He has been working at NUAA for 32 years, where he is currently the Institute Director of Air Traffic Management and the Leader of transportation planning and management. He is also the National Air Traffic Control Overall Technologist, a Member of the Expert Committee of the Ministry of Transport, a Special Expert of the Civil Aviation Administration of China, National Air Traffic Flow Management Expert, and a National Airspace Management and Assessment Expert. He has published more than 100 academic papers, one book, six patents, and five software copyrights. He has completed and is carrying out over 50 major scientific research projects and has won eight provincial and ministerial awards for scientific and technological progress.